STRESS ANALYSIS OF THE SEPARATOR IN A LITHIUM-ION BATTERY

By

Danghe Shi

A THESIS

Submitted to
Michigan State University
in partial fulfillment of the requirements
for the degree of

MASTER OF SCIENCE

Mechanical Engineering

2010

ABSTRACT

STRESS ANALYSIS OF THE SEPARATOR IN A LITHIUM ION BATTERY

By

Danghe Shi

A separator is a porous membrane that prevents the physical contact between the positive and negative electrodes while enabling ionic transport. The integrity of the separator is vital to the performance and reliability of a battery. Presently, there is no method to evaluate the stress in a separator *in situ* in a battery. In this research, a numerical model is developed to address this need. The stress in a separator is mainly caused by thermal expansion differential between battery components and lithium diffusion induced deformation in the electrodes. To compute the lithium concentration distribution and temperature change during battery operation, multi-physics models were developed in COMSOL, and then mapped to a macro-scale prismatic cell model in ANSYS. In this macro-scale model, the porous battery components were treated as homogenized media and represented with the effective properties estimated using the rule of mixtures for a composite material. The stress analysis showed that the maximum stress in the separator always emerged in the area around the inner corner where the separator wrapped around the edge of an anode and when the lithium ion battery was fully charged. Numerical simulations were also conducted to investigate the influences of three groups of design adjustable parameters on the locations and magnitudes of the maximum strain and stress of the separator. The predicted results provide the reference conditions for the improvement of separator materials and for the design of lithium ion batteries.

ACKNOWLEDGEMENTS

I would like to express my deepest gratitude to my supervisor, Dr. Xinran Xiao. She guided me onto the road of research, shared her life experience with me and instructed me to be an independent thinker. Without her guidance, encouragement, understanding and patience, it would have been impossible for me to finish this thesis. I thank everything she did for me. Many thanks also go to Dr. Soonsung Hong and Dr. Farhang Pourboghrat for their participation in the thesis committee and helpful suggestions.

I am also grateful for those people who kindly helped me throughout this research. Firstly, I would like to thank Wei Wu for her willingness to discuss on problems and share her valuable knowledge with me all the time. I puzzled over many problems with her. Secondly, I want to give a special thanks to Dr. Xiaosong Huang and Dr. H. G. Kia of General Motors Company for their support and guidance. They provided the background information for this research, and feedbacks and suggestions during the progress of this thesis. Then, I want to thank Dr. Jixing Wang and Dr. Zichao Huang for their technique support and helpful discussion. Last, I would also like to thank Samuel Goodsitt for proofreading the thesis.

I also want to express my appreciation to my friends: Fang Hou, Wenzhe Zhu, Jifeng Wang, Zi Liang, Hai Zhang, and Yalla Abushawashi. Thank them for participating in my life. Without them, it's impossible to have such wonderful and memorable life here. Finally, and most

importantly, I would like to thank my parents, my grandmother and my sister. Their endless love and support are always the most powerful driving force of my life.

This research is supported by General Motors Company under a research contract ND4306101-LT442.

TABLE OF CONTENTS

LIST OF TABLES

LIST OF FIGURES

CHAPTER 1 INTRODUCTION

Lithium-ion batteries are widely used in portable electronics such as cell phones and mobile computers. When compared with traditional batteries such as NiMH, lithium-ion technology offers superior charging efficiency, stores more energy and provides a higher discharge power density per weight and volume. The technology has been quickly advanced since its first commercial introduction in 1991 by Sony. Today lithium-ion batteries are gradually being implemented in the automotive industry with electric vehicles (EVs), hybrid vehicles (HEVs), and plug-in hybrid vehicles (PHEVs).

1.1 Lithium-Ion Battery

Lithium-ion batteries are generally composed of three primary components: anode, cathode and separator. The anode in a conventional lithium-ion battery is composed of carbon; the cathode is made of lithium transition-metal oxides or lithium metal phosphates, and the separator is synthetic polymers. All of them are placed in the electrolyte, which is a lithium salt in an organic solvent [1, 2]. Figure 1.1 is a schematic of how lithium-ion battery cells operate. Lithium, which resides within the crystal structure of the electrodes, carries current between the anode and cathode when a battery is in operation. Usually, the cell is in a discharged state when constructed. During charging, lithium ions move from the cathode through the separator to the anode. Simultaneously electrons move from the cathode to the anode through the external circuit. This process causes the potential of the cathode to rise and the anode to decrease, thus increasing the

voltage of the cell. The cell is discharged by connecting a load between the positive and negative electrodes. This causes the direction of electron and ion motion to reverse. Consequently, electrical energy is supplied to the load [3].

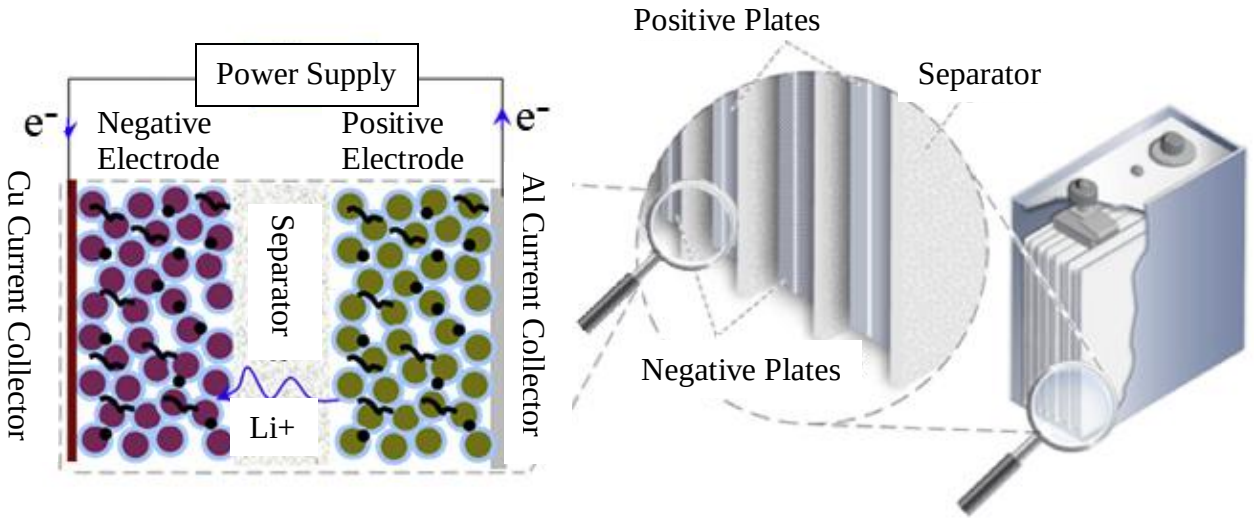

Figure 1.1 Schematic of a typical lithium-ion battery (For interpretation of the references to color in this and all other figures, the reader is referred to the electronic version of this thesis.)

Battery cells come in button, cylindrical and prismatic forms. In general, prismatic cells are custom-made for cell phones and other high volume items. For large scale applications, regardless of a cells' design, cells are packaged together into a 'module' unit; and several connected modules make up a battery pack [4]. As the first step of stress analysis of a lithium-ion battery, this thesis focuses on the stress in a separator in a prismatic cell.

1.2 Separator

Researchers of lithium-ion battery technology are mainly focused on optimizing four properties: cost, performance, safety and life. These are major technical barriers that must be addressed in

order to use lithium-ion batteries in electric vehicles and power tools. These issues, especially that of safety, become more severe as the cell sizes increase to that required to run vehicles [5]. No actual lithium-ion batteries are intrinsically safe. Short circuits due to separator failure, overcharges, over-discharges, fractures, and high temperatures can lead to thermal runaways, which may lead to fires and explosions [6]. A short circuit due to separator failure is considered to be one of the main origins of these safety problems. To prevent separator failure, one must fully understand the functionality of a separator and its working environment in a battery.

1.2.1 Functions of Separators

In production, the separators are sandwiched between positive and negative electrodes and then spirally wound together in cylindrical or folded back and forth in prismatic configurations. The pores of the separators are filled with some ionically conductive liquid electrolyte [7]. Separators are intended to prevent electronic contact, enable ionic transport between the positive and negative electrodes, provide ionic impedance at elevated temperatures, maintain good adhesion to the electrodes, and work as a reservoir for electrolyte. In order to accomplish these functions, separators must be chemically and electrochemically stable towards the electrodes and the electrolyte, and mechanically strong to withstand the high tension during the battery assembly and charge & discharge cycles during its life time [3, 7, 8].

1.2.2 Characterizations of Separators

The battery separators can be broadly divided into three categories: microporous polymer membranes, non-woven fabric mats and inorganic composite membranes. They are featured by the thinness, high porosity, and excellent thermal stability, respectively. Among them, the microporous polyolefin membranes have been most widely used in liquid electrolyte batteries due to their comprehensive advantages of performance, safety and cost [5, 8, 11].

Microporous separators have been developed from simple microporous films to complex multilayer structures in order to meet the increasing demands of high-energy batteries. The thin layers (<30μm) are made of polyethylene (PE), polypropylene (PP), or laminates of these two. Essentially PE and PP are polyolefin materials, which could provide excellent chemical stability, mechanical properties and acceptable cost to the cell [7].

The manufacturing methods of lithium-ion battery separators can be generally divided into a dry process and a wet process. Both methods include one or more orientation steps to increase porosity and improve tensile strength. Separators made by the dry process generally have slit-like pores, anisotropic mechanic properties, and relatively low tensile strength in the lateral direction. Those made by the wet process have large interconnected spherical or elliptical pores and good isotropic mechanical properties [7, 8].

The separators are wound with the electrodes under tension. They must be mechanically strong enough to withstand the tension operation during battery assembly. The mechanical strength is mainly characterized by four terms: the tensile strength along the machine direction (MD) and the transverse direction (TD), the tear resistance and the puncture strength [8]. Most of the

mechanical properties of separators can be measured or characterized by standard methods that have been established by the American Society for Testing and Materials (ASTM). Table 1.1 shows typical properties of some commercial separators.

Table 1.1 Comparison of typical properties of some commercial separators [9]

Produce name	Thickness (μm)	Porosity	Puncture Strength (g)	TD Tensile Strength (MPa)	MD Tensile strength (MPa)
Celgard 2325	25	39%	>380	14.7	166.7
Celgard C500	25	35%	>320	16.7	164.8
Celgard C300	20	36%	>300	18.1	176.5

1.3 Stress Sources in the Separator

Failure study starts from stress analysis. Stresses in separators arise from multiple sources. The first one is the deformation of the electrodes. For a typical $LiMn_2O_4$ cathode and carbon anode, the chemical reactions for cell discharging are shown as [10],

Negative electrode:

$$LiC_6 \rightarrow xLi^+ + Li_{1-x}C_6 + e^-$$

Positive electrode:

$$xLi^+ + xe^- + LiMn_2O_4 \rightarrow Li_{1+x}Mn_2O_4$$

This moving mechanism is primarily based on the diffusion processes: deliver lithium ions to the surface of the anode, transfer to and diffuse in electrolyte through the separator, and then transfer to and diffuse into the cathode [6]. The charging process proceeds in the opposite direction. The intercalation and deintercalation processes result in a volume change in the active electrode

materials, and thus the entire electrode. In a tightly packed battery, the fluctuations in the electrodes' sizes cause the separators to deform.

The second source of the stress inside a separator is temperature change. The heat generation accompanied with electrochemical reactions in a battery can be significant; this causes the battery to experience temperature rise and a thermal expansion. Since different battery components have different thermal expansion coefficients, the difference in the expansion rates induces thermal stress in the separator.

It is important to note that while stresses from a single charge and discharge operation may not be devastating, repeated stressing can initiate cracks and lead to eventual fracture of the separator.

1.4 Summary of a Literature Review

As discussed above, there is no stress directly generated inside the separator. To obtain the stress status of the separator, one should fully understand the stress behavior of the electrodes and the thermal behavior of the entire battery during operation.

There are a lot of researches focused on lithium-ion battery technologies; most of them are researched from the electrochemical point of view. Doyle et al. developed a 1-D model (or named pseudo 2-D model) of lithium-ion battery that considered the chemical performance of a full battery. In this model, each porous electrode was treated as a pseudo homogeneous mixture

of solid active material and electrolyte [12,13]. The modeling results agreed with the experimental results very well. It was used as the foundation for many later published papers.

In recent several years, researchers have started to pay attention to the stress behavior inside a lithium-ion battery during the discharging or charging process. Most of the works consider a single active particle of a spherical shape. Together with the pseudo 2D battery model, a 1D spherical model can describe the generation of stress during intercalation and deintercalation. Christensen and Newman studied the stress generated inside $LiMn_2O_4$ [14] and carbon [15] electrodes. Zhang et al. considered stress effect on diffusion and the stress distribution inside one single electrode particle using numerical simulation [16]. Cheng and Verbrugge compared the stress evolution process under galvanostatic and potentiostatic operation [17], and studied the effects of surface tension and modulus on diffusion induced stress within spherical nonoparticles [18]. Verbrugge and Cheng [19] also examined the stress in spherical particles under periodic potential excitations. Renganathan et al. [20] considered the stress arising due to the phase transformation in their model. Golmon et al. [21] presented a multi-scale finite element approach to study the electrochemical-mechanical interaction phenomena at macro-, meso-, and micro-scales.

It is well recognized that the material property of battery components will vary with temperature and lithium concentration. However, due to the complexity of the problem and lack of data, the material property was treated as constant in most of the studies. Recently Cai and White [22] considered the temperature dependence of the diffusivity, open circuit potential, and thermal conductivity.

Although most of the stress analysis was limited to one single particle, 2D models have appeared in literatures. Garcia et al [23] developed a 2-D model to study the effects of distribution change or size change of the particles, meanwhile considered more details of the microstructure of the electrode. Xiao et al. [24] developed a multi-physics, multi-scale model for a lithium-ion battery in a multi-physics code COMSOL taking into account the reaction kinetics, lithium diffusion and diffusion induced stress. Unfortunately, due to the limitation of the COMSOL in its structural module, the development of a robust model with contact between the battery components was not successful and a continuous mesh had to be used across the components. The stress calculated by this approach may represent the condition in the center of a cell but not at the electrode edges. To consider the contact between battery components, a structural code with a robust contact modeling capability is needed.

As to the thermal behavior of a lithium-ion battery, although several studies have addressed the issue of heat generation inside lithium-ion batteries [25-27], most works were conducted to describe the heat generation, temperature change or their influence on certain electrochemical properties, few researches have considered the thermally induced stress. As an extension of Xiao's work, Wei et al. [28] introduced thermal stress in 2-D lithium-ion battery model. The results showed that, for the separator, the influence of the thermal stress were as important as that of lithium diffusion induced stress.

1.5 Scope of the Work

It is well recognized that stress can have a significant impact on the performance of a separator. Currently, there is no method to evaluate the stress inside a battery. There are no clear criteria for the mechanical property requirement of the separators. To improve the performance of battery separators, their stress conditions must be known.

The objective of this research is to develop a numerical model for the stress analysis of the separator in a prismatic lithium ion battery cell. A prismatic cell is commonly known as a pouch cell.

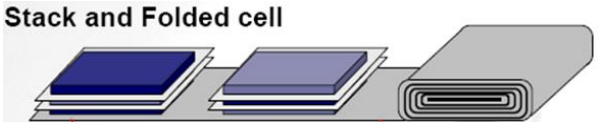

Figure 1.2 Schematic of a pouch cell [29]

A pouch cell is manufactured by stacking up layers of electrodes separated by separator films. Figure 1.2 presents the schematic of a pouch cell [29]. The actual stacking and folding configuration in batteries may vary. It is expected that the stress in a separator is higher near the edge than in the center.

Limited by the availability of the data and understanding on the multi-physics processes in lithium-ion batteries, the following assumptions are made at this stage of the work:

1) All materials are linear elastic and isotropic.
2) Material properties are considered to be independent of lithium concentration.
3) Material properties are considered to be independent of temperature.

4) The solid phase of electrode is assumed to only consist of active particles. The binders and other additives are neglected.
5) The effects of stresses on electrochemical reactions and lithium diffusion are ignored.

1.6 Scope of the Thesis

This work is generally divided into two parts: the development of numerical models and the study of the influence of some design adjustable parameters.

Chapter 1 provides the background information about this research, describes the objective and scope of this work, and presents the organization of this thesis.

Chapter 2 introduces the main phenomena occurred inside the lithium-ion battery, and provides the corresponding governing equations and the coupling relationships between various physical phenomena.

Chapter 3 describes the lithium-ion battery model developed in this research and provides a summary of the input parameters in the models. To consider the porosity of porous components, a homogenization technique was used to obtain the effective properties and is discussed in this chapter. In this thesis, a model for the stress analysis of a separator is developed based on two commercial softwares: COMSOL and ANSYS. The way to use these two commercial softwares is discussed at the end of this chapter.

Chapter 4 presented the simulation results. In this chapter, several important factors of a lithium-ion battery are studied. The influences of each factor to the stress condition of the separator are summarized. A series of optimized parameters are suggested at the end of this chapter.

Chapter 5 summarized the major findings in this work and suggested some directions for the future work.

CHAPTER 2 METHODS

As introduced in Chapter 1, there are three major groups of phenomena occurring inside a lithium-ion battery: electrochemical, thermal and mechanical phenomena. Since they are strongly related to each other, they will be investigated as coupled phenomena in order to accurately and systematically analyze the stress. This chapter will introduce the basic equations that used to describe these phenomena and discuss the coupling methods.

2.1 Multiple Phenomena Occurred inside the Lithium-Ion Battery

The phenomena occurred inside the lithium-ion battery can be generally classified into three groups: electrochemical phenomena, thermal phenomena and mechanical phenomena. Each group is described by a different set of equations. The electrochemical reactions serve as the foundation for all these analysis.

2.1.1 Electrochemical Phenomena

It has been proved that the multiple electrochemical phenomena inside a lithium-ion battery can be described by a set of mathematical equations. Detailed mathematical models have already been established by Doyle et al. [12, 13]. It was proved that the simulation results predicted by these models match with experimental results very well. In this study, the analysis of electrochemical phenomena is built upon these well established mathematical models.

2.1.1.1 Current Balance

In the solid phases of the electrodes, the current balance is described in terms of electronic current density balance

$$\nabla(-\kappa_{1\_i,eff}\nabla\phi_{1\_i}) = -S_{a\_i}\, j_{loc\_i} \qquad (2.1)$$

where i=p,n, p denotes positive electrode, n denotes negative electrode, $\kappa_{1\_i,eff}$ denotes the effective electronic conductivity, φ_{1_i} is the potential of the solid electrode, S_{a_i} refers to the specific surface area (m^2/m^3) , j_{loc_i} is the local charge transfer current density. Equation 2.1 also represents the conservation of charge in the solid phase. The effective conductivity considers porosity and tortuosity, the expression is given by

$$\kappa_{1\_i,eff} = \kappa_{1\_i}\varepsilon_{1\_i}^{\gamma} \qquad (2.2)$$

where κ_{1_i} is the electronic conductivity, ε_{1_i} is the volume fraction of solid phase, γ is the Bruggeman coefficient, which is set to 1.5 in this work.

In electrolyte phase, the current balance denotes the ionic charge balance. The equation for binary 1:1 electrolytes can be given as

$$\nabla(-\kappa_{2\_i,eff}\nabla\phi_{2\_i}) + \nabla(-\kappa_{D\_i,eff}\nabla\ln c_{2\_i}) = S_{a\_i}\, j_{loc\_i} \qquad (2.3)$$

where φ_{2_i} is the potential of electrolyte, c_{2_i} is the salt concentration in electrolyte, $\kappa_{2\_i,eff}$ is the effective electronic conductivity, the expression is

$$\kappa_{2\_i,eff} = \kappa_{2\_i}\varepsilon_{2\_i}^{\gamma} \qquad (2.4)$$

where κ_{2_i} is the electrolyte ionic conductivity, which strongly depend on the electrolyte composition. In this work, Newman's experimental data was used, as shown in Figure 2.1. ε_{2_i} is the volume fraction of electrolyte (porosity).

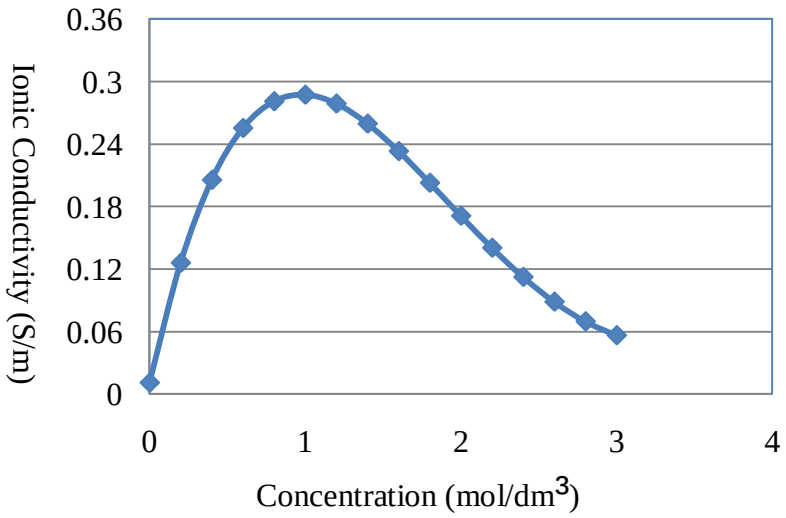

Figure 2.1 Relationship between ionic conductivity and lithium concentration in electrolyte

$\kappa_{D\_i,eff}$ is the diffusional conductivity, which is given by

$$\kappa_{D\_i,eff} = \frac{2RT\kappa_{2\_i,eff}}{F}(1+\frac{\partial \ln f}{\partial \ln c_{2\_i}})(1-t_+) \qquad (2.5)$$

where R denotes the gas constant, T denotes the temperature, f is the ionic activity coefficient, and t_+ is the transference number of the Li^+ with respect to the velocity of solvent. In this work, we assume the ionic activity coefficient does not change with the salt concentration, thus, the diffusional conductivity can be rewritten as

$$\kappa_{D\_i,eff} = \frac{2RT\kappa_{2\_i,eff}}{F}(1-t_+) \qquad (2.6)$$

2.1.1.2 Material Balance in the Electrolyte

The material balance in the electrolyte is given by

$$\varepsilon_{2\_i}\frac{dc_{2\_i}}{dt}+\nabla(-D_{2\_i,eff}\nabla c_{2\_i})=\frac{S_{a\_i}j_{loc\_i}}{F}(1-t_{+}) \qquad (2.7)$$

where $D_{2\_i,\mathrm{eff}}$ is the effective diffusion coefficient in the electrolyte, which is calculated in the same way as we do for effective conductivity.

2.1.1.3 Diffusion in the Solid Electrode Particles

Fick's second law describes the transport in the solid electrode particles and predicts the change of concentration field with time by the following equation in spherical coordinates

$$\frac{dc_{1\_i}}{dt}+\frac{1}{r^2}\frac{\partial}{\partial r}[-r^2D_{1\_i}\frac{\partial}{\partial r}(c_{1\_i})]=0 \qquad (2.8)$$

where c_{1_i} is the concentration of species in solid electrode.

2.1.1.4 Butler-Volmer Electrode Kinetics [10, 25]

Butler-Volmer electrode kinetics describes the fundamental relationship between electrical current on an electrode, the electrode potential and the local specie concentration at the interface between electrode and electrolyte. In particular, the rate of transfer of lithium ions from the electrolyte to the active material is controlled by the local deviation of the surface potential with

respect to its equilibrium value. It serves as the link term between charge balance and material balance. The Butler-Volmer relation is given as

$$j_{loc\_i} = \frac{i_{0\_i}}{F}\{\exp[\frac{(1-\beta)F\eta_i}{RT}] - \exp[\frac{-\beta F\eta_i}{RT}]\} \qquad (2.9)$$

where i_{0_i} is the exchange current density, η_i is surface overpotential, and β is the symmetric factor, which represents the fraction of the applied potential that promotes the cathodic reactions[25]. The first term in the brace denotes the forward rate of the anodic process, while the second term denotes the backward rate of the cathodic process [23]. The exchange current density is given by

$$i_{0\_i} = Fk_{0\_i}(c_{2\_i})^{1-\beta}(c_{1\_i,\max} - c_{1\_i,surf})^{1-\beta}(c_{1\_i,surf})^{\beta} \qquad (2.10)$$

where k_{0_i} is the reaction rate constant, c_{2_i} is the concentration of lithium ion in the electrolyte, $c_{1\_i,surf}$ is the concentration of lithium ion on the surface of the solid electrode, and $(c_{1\_i,max} - c_{1\_i,surf})$ is the available space for lithium intercalation. The overpotential is given by

$$\eta_i = \phi_{1,i} - \phi_{2,i} - U_i \qquad (2.11)$$

where $\phi_{1,i}$ is the potential of the solid electrode, $\phi_{2,i}$ is the potential of the electrolyte, and U_i is the open circuit potential, or the electrode particle's equilibrium potential, which is a function of the state of charge. It can be measured by experiment. In this work, the experimental results from Reference 13 were used.

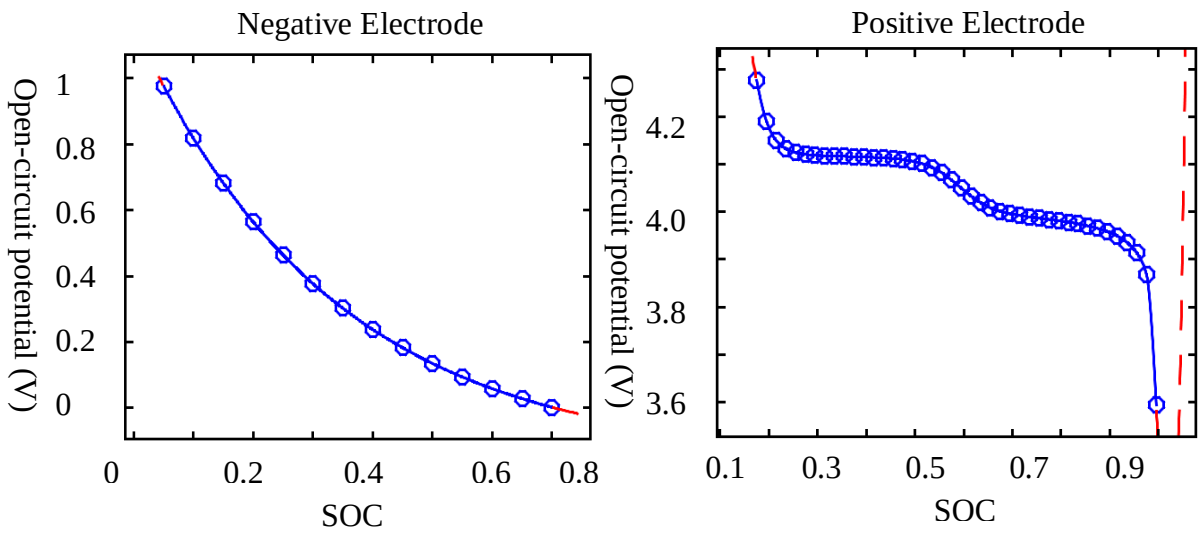

Figure 2.2 OCP of negative electrode and positive electrode [13]

The boundary conditions for electrochemical reactions are presented in Appendix A.

2.1.1.5 Initial Conditions

The initial concentrations of lithium in each component that used in the simulation of the electrochemical reactions are listed in Table 2.1.

Table 2.1 Initial species concentration

	Anode (mol/m^3)	Separator (mol/m^3)	Cathode (mol/m^3)
In Electrolyte	2000	2000	2000
In solid Electrode	5000	--	20500

2.1.2 Thermal Phenomena

Battery thermal management is a critical element for achieving the desired performance and calendar life for battery packs. According to Wu et al. [28], the thermal stress imposed on the separator due to the self-heating of the battery is substantial. To understand the stress behavior of a lithium-ion battery, the self-heating of the battery must be considered.

To understand the thermal behavior of a lithium-ion battery, we introduced the energy balance, given by [26, 30]

$$\rho_i C_{p\_i} \frac{\partial T}{\partial t} = \nabla \cdot (\lambda_i \nabla T) + q_i \qquad (2.12)$$

where from left to right, the terms denote heat accumulation, heat conduction and heat generation. For heat generation, there are mainly four sources [25, 28], which can be written as

$$q_i = s_a j_{n\_i} (\phi_1 - \phi_2 - U_i) + s_a j_{n\_i} T \frac{\partial U_i}{\partial T} + \sum_k \Delta H_k^{avg} r_k + \int \sum_r \sum_s (\overline{H}_{rs} - H_{rs}^{avg}) \frac{\partial c_{rs}}{\partial t} dv \qquad (2.13)$$

where s_a is the specific surface area (m^2/m^3), j_{n_i} is the current density (A/m^2). The first term is the irreversible resistive heat, represents the deviation of the cell potential from its equilibrium potential; the second term is the reversible entropy heat; the third term is the chemical side reaction heat, and the fourth term is the heat of mixing due to the generation and relaxation of concentration gradients. As revealed in Reference 27, the heat of mixing is relatively small compared to entropic and resistive heat, thus it can be neglected. In this study, a binary electrolyte is assumed; side reactions and phase change effects are neglected. The energy balance equation reduced to

$$\rho_i C_{p\_i} \frac{\partial T}{\partial t} = \nabla \cdot (\lambda_i \nabla T) + s_a j_{n\_i} (\phi_1 - \phi_2 - U_i) + s_a j_{n\_i} T \frac{\partial U_i}{\partial T} \qquad (2.14)$$

Experimental results of $\partial U/\partial T$ for $LiMn_2O_4$ [31] and LiC_6 [10, 32] are used in this study as shown in Figure 2.3.

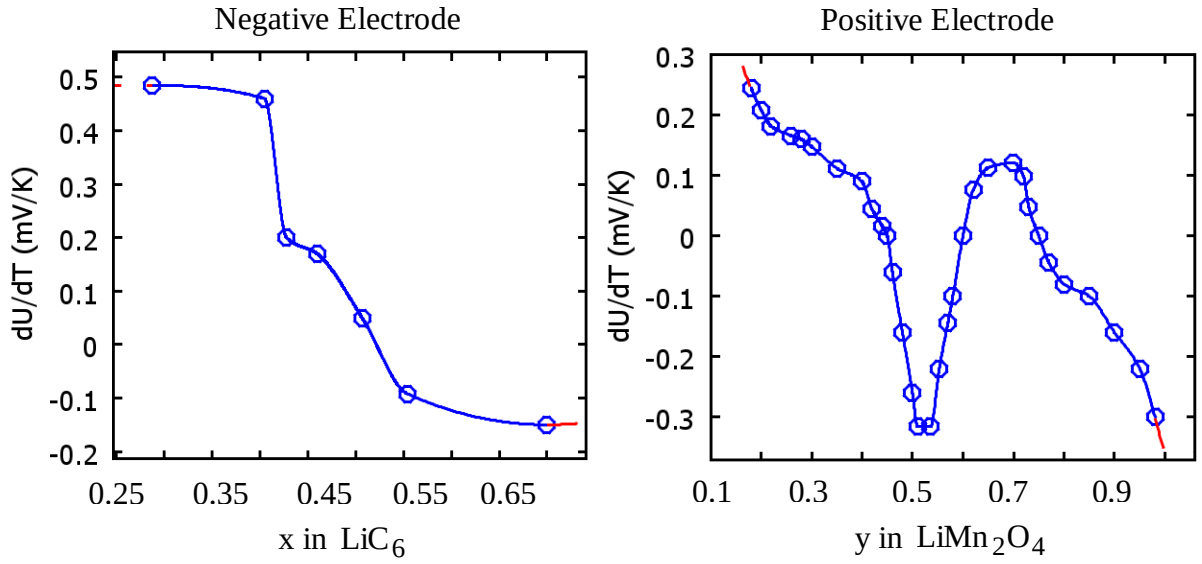

Figure 2.3 $\partial U/\partial T$ for anode (LiC_6) and cathode ($LiMn_2O_4$)

The thermal boundary conditions are shown in Chapter 3.

2.1.3 Mechanical Phenomena

Linear elasticity is assumed in this research, and the Young's modulus is treated as a constant. Therefore the strain would always vary proportionally with the stress. Besides the conventional mechanical strain, thermal strain and diffusion induced strain also arise in lithium-ion batteries [16, 24, 33]. The constitutive relationship can be written as:

$$\varepsilon_{ij} = \varepsilon_{ij}^{me} + \varepsilon_{ij}^{ei\_T} + \varepsilon_{ij}^{ei\_c} = \frac{1}{E}((1+\nu)\sigma_{ij} - \nu\sigma_{kk}\delta_{ij}) + \alpha_{ij}\Delta T\delta_{ij} + \frac{1}{3}\Delta c\Omega\delta_{ij} \qquad (2.15)$$

where ε_{ij} are strain components, E is Young's modulus, ν is Poisson's ratio, σ_{ij} are stress components, δ_{ij} is the Kronecker delta, α_{ij} is thermal expansion coefficient, ΔT is the temperature change from the reference value, Δc is the concentration change of diffusion species from the reference value, and Ω is the partial molar volume. The partial molar volume can be calculated by [24]:

$$\Omega = \frac{3\varepsilon}{\Delta y c_{\max}} \tag{2.16}$$

where ε is the intercalation induced strain along the major axis of the material, Δy is the change of number of lithium atoms, and c_{max} is the Stoichiometric maximum concentration.

The mechanical boundary conditions are discussed in Chapter 3.

2.2 Multi-physics Coupling

The previous analysis has already shown that there are mainly two sources of stress in a separator: lithium diffusion induced stress and thermal stress. Therefore the lithium and temperature distribution are needed to perform stress analysis. In this work, the simulation is divided into two steps: 1) obtain the lithium and temperature distributions using COMSOL, 2) perform stress analysis in ANSYS. This is a one way coupling method. The influences of stress on the lithium and temperature distributions are neglected.

2.2.1 Lithium and Temperature Distributions

The lithium distribution is predicted by a 1-D cross section model and the temperature distribution is predicted by a macro-scale 2-D model. Both models are coupled with pseudo 2-D battery models in COMSOL.

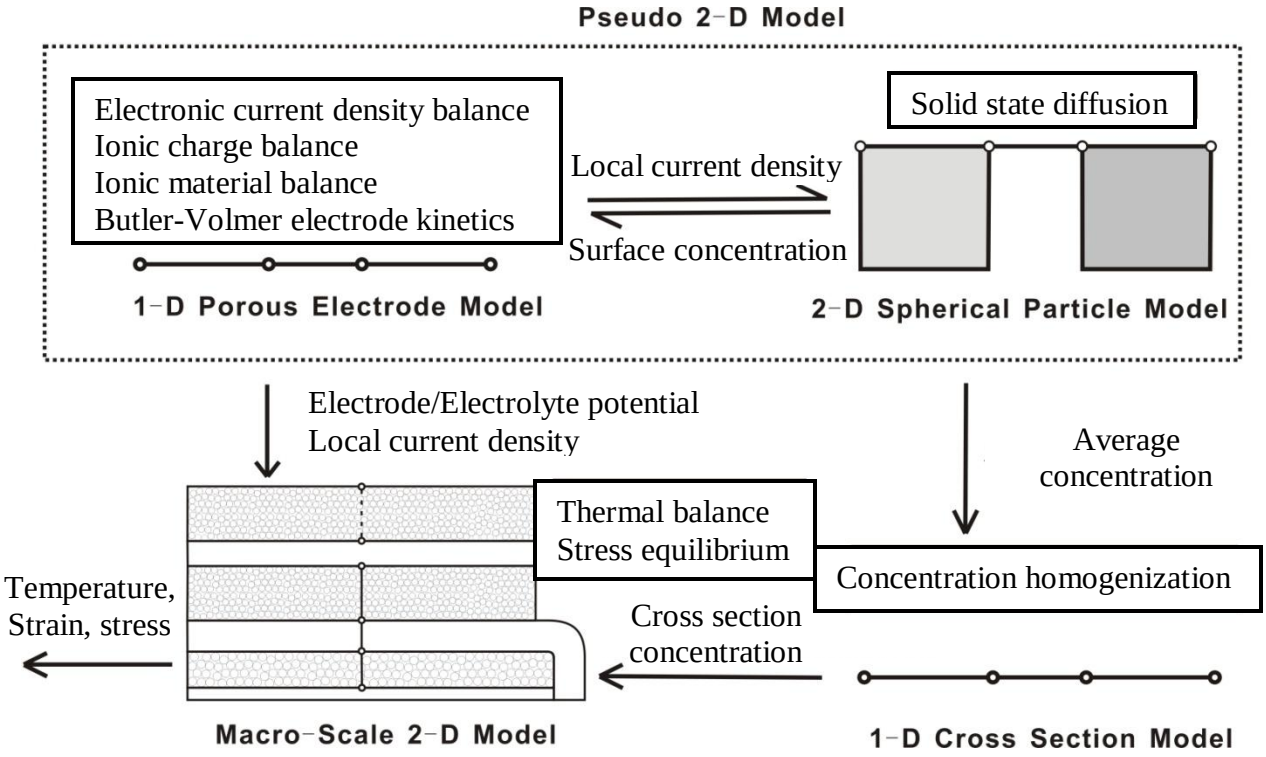

Figure 2.4 Schematic of multiphysics coupling

As shown in Figure 2.4, the first two models are called pseudo 2-D battery models (available in COMSOL 3.5a), which was built upon the model developed by Doyle et al. [12, 13]. The pseudo 2-D model consists of a 1-D porous electrode model and a 2-D spherical particle model. Generally the 1-D porous electrode model deals with the electronic current density balance, ionic charge balance, ionic material balance, and Butler-Volmer electrode kinetics, while the 2-D spherical particle model provides the lithium concentration distribution inside the particles and the lithium concentration at the particle surface for the 1-D porous electrode model.

Xiao et al. developed a multi-scale model of a lithium-ion battery [24]. In this model, while lithium ions inside the electrode were redistributed, the stress inside the separator did not change during the relaxation time in a charge-discharge cycle. Therefore, the distribution of lithium ions inside the electrodes does not affect the stress inside the separator. Based on this finding, in order to simplify modeling, lithium inside each particle is assumed to be evenly distributed. Under this assumption, the lithium concentration profile along any cross section in the macro-scale 2-D model can be treated as the same; or it only varies along the thickness of the electrodes.

The cross section distribution of lithium ions is obtained by projecting the distribution of the 2-D spherical particle model into a 1-D cross section model. Each point of the 1-D cross section model represents the average concentration value of a sphere particle derived from the corresponding line in the 2-D spherical particle model. The average lithium concentration inside a particle is calculated by:

$$c_{ave} = \frac{1}{\frac{4}{3}\pi r^3}\int_0^r 4\pi r^2 c_1 dr = \frac{3}{r^3}\int_0^r r^2 c_1 dr \tag{2.17}$$

In the 2-D spherical particle model, $y = \frac{r}{r_i}$, $y \in [0,1]$, the equation can be rewritten as:

$$c_{eff\_i} = 3\int_0^1 c_1 y^2 dy \tag{2.18}$$

where c_{eff_i} is the average concentration of lithium in the i^{th} electrode in the 1-D cross section model, c_1 is the concentration of lithium along the radius in the 2-D spherical particle model. The 1-D cross section model represents the cross section of the macro-scale 2-D model. The concentration of lithium in the macro-scale 2-D model can be obtained by extruding the

concentration values in the 1-D cross section model along the length of the macro-scale 2-D model as shown in Figure 2.5.

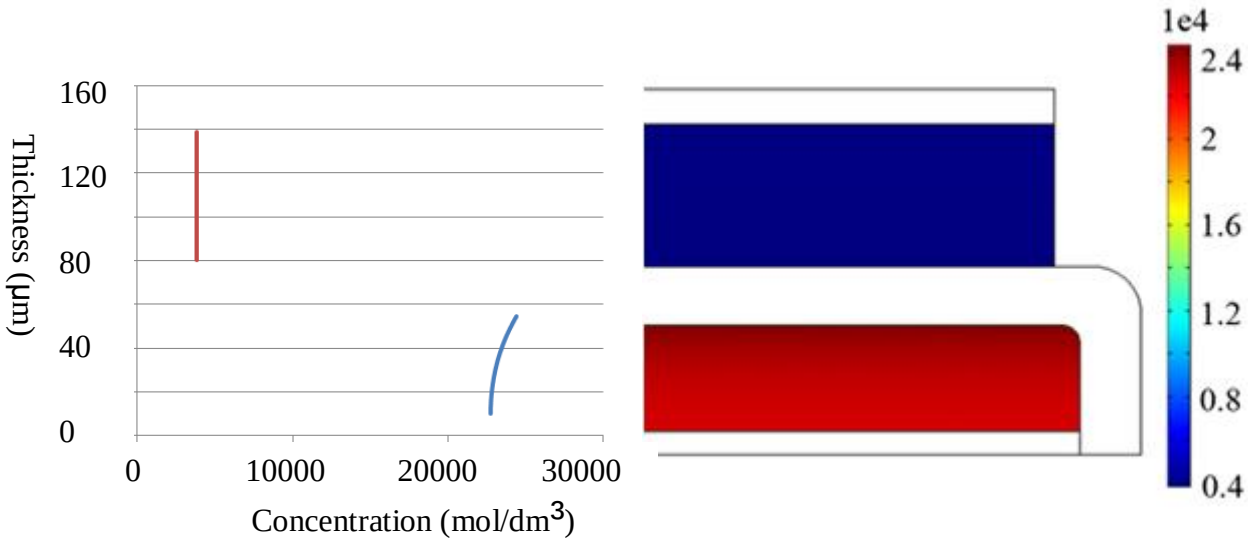

Figure 2.5 Lithium distributions in the real 2-D model

After obtaining the concentration distribution, a thermal analysis can also be performed on the macro-scale 2-D model. As presented in equation 4, variables, such as current density and potential, are needed in addition to the lithium ion concentration in order to perform this thermal analysis. These variables are directly projected from the 1-D porous electrode model.

2.2.2 Stress Analysis

After solving the strongly coupled electrochemical and thermal equations, the lithium and temperature distributions are successfully extracted. The extracted distributions are used as input for the macro-scale 2-D model and the stress analysis of the battery is performed subsequently in ANSYS.

CHAPTER 3 MODEL

In this study, we are interested in one cell of a prismatic lithium-ion battery. As introduced in Chapter 1, each cell of the battery is composed of parallel layers of different components. The stress at the middle part of the prismatic battery would converge to a stable value, but the stress at the end of the battery could change greatly due to different wrapping methods of the separator and actual shapes of the corners of the electrodes.

There are two ways to wrap the separator: wrap around the anode or wrap around the cathode. In this thesis, an assumption, to be introduced in Chapter 4, is made that all lithium ions which participate in reaction come from the cathode. Under this condition in one charge & discharge cycle, deformation induced by lithium diffusion causes the cathode to first shrink and then expand back to its original shape, and the anode to act in an opposite manner. Therefore, only the separators wrapped around the anode are expected to experience high strain and stress fluctuations. The addition of thermal expansion under these conditions will reduce stress and strain regardless of the wrapping method. Since this research is aimed at determining the maximum stress imposed on the separator, we mainly focus on the methods of wrapping the separator around an anode.

The shape of the corner may change according to different assembly methods. For the model in this research, the separator is wrapped tightly enough around the anode that the transition area

(corner) is considered to be annulus. This maximum stress yields from this model can be considered the lowest value when compared with other possible conditions.

3.1 Model Depiction

3.1.1 Structure and Dimensions

The stress condition of a separator is closely related to material properties, the diffusion of lithium, heat change, the actual stacking and folding configuration of the electrode assembly, and the packing of the battery. In this research, all these conditions are finally exerted on a macro-scale 2-D model. The macro-scale 2-D model is a representative 1.5 cell model as shown in Figure 3.1. The model is regularly shaped with smooth surfaces. The components from the bottom to the top are anode current collector (Cu), anode, separator, cathode, cathode current collector (Al), and another cathode. The separator is wrapped around the anode and assembled tightly with both the anode and the cathode.

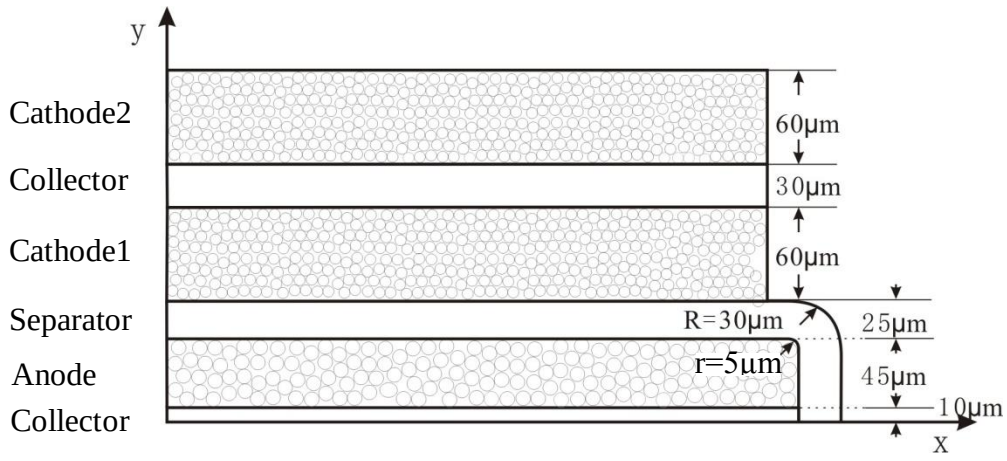

Figure 3.1 Schematic of the structure of the model

It's important to note that a 1.5 cell model is built in this study instead of one full cell. If only one full cell is modeled, one layer of cathode and one layer of collector would form an asymmetric beam which tends to bend under diffusion induced stress in cathode layer and to peel off from the separator. In reality, since the collector is coated with cathode layers on both sides, the bending forces will be counteracted by each other. To represent this real condition, one needs to add another cathode into the full cell model, and therefore a 1.5 cell model is formed. The collector for the anode is coated at both sides as well. This is represented by a symmetrical boundary condition at the lower surface of the current collector in the model. The boundary condition will be discussed. The dimensions of the model are listed in Table 3.1.

Table 3.1 Dimensions of the model

		Unit	Cu	Anode	Separator	Cathode	Al
Particle radius		μm		11.5[34]*		3.35[35]	
Thickness		μm	10	45	25	60	15
Length**		mm	7	7	7.025	6.98	6.98
Corner	Inner	μm			5		
radius	Outer	μm		5	30		

*Estimated as the value of r50.
**Effective length. Its effectiveness is verified by numerical experiment in Chapter 4.

3.1.2 Boundary Conditions

Assigning proper boundary conditions to approximate the real conditions is critical to obtain a correct solution for the problem. In this study, three groups of phenomena are investigated and thus there are three sets of boundary conditions for different governing equations and simulation models. As introduced in Chapter 2, the pseudo 2-D models are used to deal with electrochemical reactions. The boundary conditions for them are presented in Appendix A. The

macro-scale real 2-D model is used to deal with both thermal and mechanical phenomena. The boundary conditions for these phenomena are illustrated in Figure 3.2 and Figure 3.3.

Figure 3.2 presents the thermal boundary conditions of the macro-scale 2-D model. We assume that for the right hand side boundaries, heat transfer with air is achieved by blowing the air along the thickness of the cell; thus, a convective boundary condition is assigned to the right hand side boundaries. For all the other sides, an adiabatic boundary condition is applied because of the symmetric conditions. Inside the lithium-ion battery, heat can conduct freely from one component to another; therefore, free conductive boundary conditions are applied for all the inner boundaries.

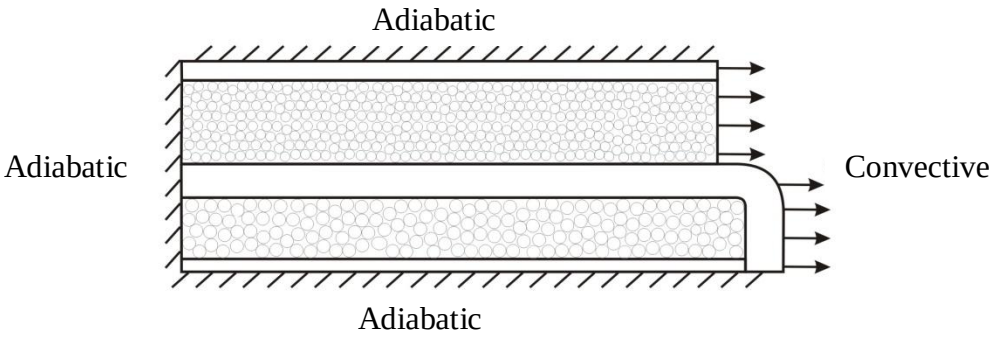

Figure 3.2 Thermal boundary conditions

Figure 3.3 is the schematic of the mechanical boundary conditions of the macro-scale 2-D model. Similarly, there are two groups of boundaries in this model: external and internal. For the external boundaries, a symmetric displacement boundary condition is assigned to the left and bottom boundaries, thus the model we study represents one quarter of 3.0 full cells. Distributed normal pressure is assigned to the top boundary. The default value for this pressure is 10 psi.

This value may change when conducting a pressure study in Chapter 4. The rest of the external boundaries are free boundaries.

To set the internal boundary conditions, one needs to consider the production process of battery cells. At the beginning of the production process, a cathode paste is spread on Al foil (cathode collector) and an anode paste is spread on Cu foil (anode collector), therefore the electrodes and their corresponding collectors are always bonded together. Then, these bonded components are wounded up sequentially with separators [4]. Relative slip can occur on the surfaces between a separator and its adjacent electrodes. Due to this production process a contact relationship is assigned at the boundaries between the separator and electrodes in the model; and the boundaries between the current collector and the electrode are modeled as continuous.

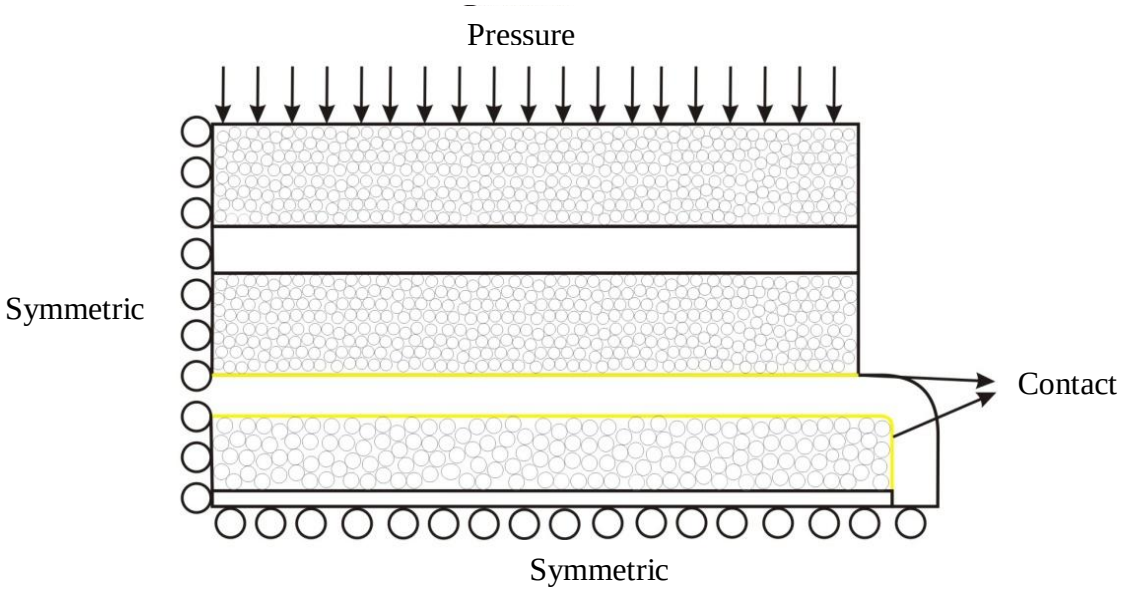

Figure 3.3 Schematic of mechanical boundary conditions for the real 2-D model

3.2 Material Properties

Anodes for lithium-ion batteries can be made of lithium, carbon, lithium-alloying materials, intermetallics, or silicon. Among these, carbon is selected as the anode materials. Carbon is the common anode in commercial lithium-ion batteries due to its popularity as being a low cost and highly available material [6, 36]. The corresponding current collector is Cu foil.

Materials used in cathodes in lithium-ion batteries include lithium-metal oxides (like $LiCoO_2$, $LiMn_2O_4$, and $Li(Ni_xMn_yCo_z)O_2$), vanadium oxides, olivines or rechargeable lithium oxides [36, 37]. In this research, the material considered is $LiMn_2O_4$. Manganese offers a low-cost substitution with a high thermal threshold and excellent rate capabilities [6]. The material parameters for $LiMn_2O_4$ are well established. The corresponding current collector is Al foil.

In lithium-ion batteries the electrolyte is made of a solution of a fluorinated lithium salt in an organic solvent, which enables current to transport by lithium ions. The solvent-based electrolytes generally contains $LiBC_4O_8$ (LiBOB), $LiPF_6$, $Li[PF_3(C_2F_5)_3]$ [6]. We choose $LiPF_6$ (hexafluorophosphate) as the lithium salt.

As introduced before, the separator considered in this work is a microporous film made by a wet process.

Overall, a $Cu/Li_yC_6/LiPF_6/Li_yMn_2O_4/Al$ cell has been selected in this research. All the materials are the most common materials used in each corresponding component of lithium-ion batteries.

3.2.1 Effective Property

As shown in Figure1.1, the separator and electrodes are porous. All the pores are filled with electrolytes. However, in this research, each component is modeled as a homogeneous solid medium. The materials' porosity is taken into consideration by applying effective properties. This study is focused on the stress in the separator. It is assumed that, when observed macroscopically, the local details of the electrodes will not contribute significant influence on the stress in the separator, as long as the equivalent macroscopic strains of the electrodes are generated. In other words, the same macroscopic behavior can be achieved by applying the Rule of Mixture to each material property used in the equations.

3.2.1.1 Diffusion and Thermal Induced Expansion Coefficient

Each component can be treated as a compound of the local material and electrolyte. In this study the electrolyte is considered to be compressible, but its volume variation due to Li+ concentration change is assumed to be negligible. Only the electrode particles experiences lithium diffusion induced volume change. To account for this influence, an effective diffusion expansion coefficient is estimated. The diffusion induced expansion coefficient is estimated by the rule of mixtures similar to composite systems as [38]

$$\beta_{eff} = \sum_i \beta_i V_i = \sum_i \frac{1}{3} \Omega_i V_i \tag{3.1}$$

where β_{eff} is the effective diffusion expansion coefficient of the composite, β_i and V_i are the diffusion induced expansion coefficient and the volume fraction of the i^{th} phase, respectively. Neglecting the contribution of the electrolyte phase, the expression can be reduced to

$$\beta_{eff} = \beta_p V_p = \frac{1}{3}\Omega_p V_p \tag{3.2}$$

where β_p and V_p are the diffusion induced expansion coefficient and the volume fraction of the active particles, respectively. With this effective diffusion expansion coefficient, the macroscopic equivalent strain of an electrode due to lithium insertion and extraction can be obtained.

The effective thermal expansion coefficient of the electrode was estimated in the same way, but the expansion of the electrolyte cannot be neglected. It is defined as:

$$\alpha_{eff} = \sum_i \alpha_i V_i \tag{3.3}$$

where α_{eff} is the effective thermal expansion coefficient of the composite, α_i is the diffusion induced expansion coefficient of the i^{th} phase.

3.2.1.2 Thermal Conductivity and Specific Heat Capacity

The method used to obtain the effective thermal conductivity and specific heat capacity is very similar to the one for expansion coefficients. It is important to ensure the overall performance is still the same. The effective thermal conductivity can be calculated by:

$$k_{eff} = \frac{\sum_i k_i L_i}{\sum_i L_i} \approx \frac{\sum_i k_i \sqrt[3]{V_i}}{\sum_i \sqrt[3]{V_i}} \tag{3.4}$$

where k_{eff} is the effective thermal conductivity of the composite, k_i is the thermal conductivity of the i^{th} phase, L_i is the conduct length.

The effective specific heat capacity can be calculated by:

$$c_{p\_eff} = \frac{\sum_i c_{p\_i} m_i}{\sum_i m_i} = \frac{\sum_i c_{p\_i} \rho_i V_i}{\sum_i \rho_i V_i} \tag{3.5}$$

where c_{p_eff} is the effective specific heat capacity of the composite, c_{p_i} is the specific heat capacity of the i^{th} phase, m_i is the i^{th} mass fraction, ρ_i is the density of the i^{th} phase.

3.2.1.3 Young's Modulus

Similarly, the Young's modulus of a porous electrode is different from that of an electrode particle. The effective modulus of a composite consisting of particles dispersed in a matrix is found to fall between the following upper and lower bounds, respectively.

$$\text{Upper bound: } E_{eff} = E_m V_m + E_p V_p \tag{3.6}$$

$$\text{Lower bound: } E_{eff} = \frac{E_m E_p}{V_m E_p + V_p E_m} \tag{3.7}$$

where E_{eff} is the effective Young's modulus of the composite, E_m and E_p are the Young's modulus of the matrix and particles, respectively [38, 39]. The mass fraction of the active

materials in electrodes is assumed to be 0.8 [40]. From the mass fraction and densities of battery components, the computed volume fractions of the active materials are 0.69 for the carbon anode and 0.53 for the $LiMn_2O_4$ cathode. At a high particle volume fraction, the upper bound estimation provides a closer approximation. Therefore, the prediction found with Equation (3) was used in this work to calculate the effective Young's modulus.

3.2.2 Material Constants

Table 3.2 lists a summary of the material constants and the effective values of some modified parameters of different battery components.

Table 3.2 Material property of different components in a lithium-ion battery

Electrochemical Constants

	Unit	Cu	Anode	Separator*	Cathode	Al	Electrolyte
Density	kg/m^3	8700	2223	900	4202	2700	1210
Stoichiometric maximum concentration	mol/m^3		$2.64x10^4$ [13]		$2.29x10^4$ [13]		
Initial SOC			0.227		0.612		0.200
Diffusion coefficient	m^2/s		$3.9x10^{-14}$		$7.08x10^{-15}$		
Partial molar volume	m^3/mol		$4.17x10^{-6}$		$3.5x10^{-6}$		
Effective Partial molar volume	m^3/mol		$2.88x10^{-6}$		$1.86x10^{-6}$		
Porosity			0.26	0.42[7]	0.407		
Active volume fraction			0.69		0.53		

Thermal Constants

	Unit	Cu	Anode	Separator	Cathode	Al	Electrolyte
Thermal expansion coefficient	1/K	$17x10^{-6}$	$4.06x10^{-6}$	$13.32x10^{-5}$	$8.62x10^{-6}$	$23.6x10^{-6}$	$12.4x10^{-6}$
Effective Thermal expansion coefficient	1/K		$6.025x10^{-6}$	$82.46x10^{-6}$	$9.615x10^{-6}$		
Specific heat capacity	J/kg*K	386	623	1883	672	897	1800
Effective specific heat capacity	J/kg*K		823		839[41]		
Thermal conductivity	W/m*K	398	6.5	2.16	6.2	237	0.099
Effective thermal conductivity	W/m*K		3.81		3.28		
Heat transfer coefficient of air	W/m^2*K	5					

Mechanical Constants

	Unit	Cu	Anode	Separator	Cathode	Al	Electrolyte
Young's modulus	GPa	117	12	0.5	10	70	1MPa[23]
Effective Young's modulus**	GPa		8.88		5.93		
Poisson's ratio		0.35	0.3	0.35	0.3	0.34	0.25[23]

* All the data of separator are calculated by using wet separator, no effective values are needed.

** All the none-electrolyte parts are treated as solid particles.

CHAPTER 4 SIMULATION

4.1 Simulation Conditions

In this thesis, research is focused on the strain and stress of a separator at the end of a charging period of the $Cu/Li_yC_6/LiPF_6/Li_yMn_2O_4/Al$ battery. Charging procedures are composed of two steps: charge the battery at constant current until reaching a voltage of 4.2 V, and then hold the cell voltage at 4.2 V while gradually reducing the charging current until it drops to a small percentage of the initial charge rate, such as 3%. At this point, the battery is considered to be fully charged [42].

In this study, the lithium ion concentration is expressed in state of charge (SOC), which is the ratio of the current lithium ion concentration to the battery's Stoichiometric maximum concentration. The initial stresses in all battery components are assumed to be zero. Thus, the stress free conditions are the conditions of the battery before the first charge. As shown in Table 4.1, based on the assumption that all lithium ions come from the cathodes, the stress free SOC is 0 for anodes. The initial SOC is calculated from Table 2.1.

Table 4.1 Assumed SOCs for both electrodes

	Stress free SOC	Initial SOC
Anode	0	0.208
Cathode	0.98	0.919

Due to the cyclical nature of rechargeable batteries, initial charging conditions match the final conditions of discharge. In operation cycles, the degree of discharge (DOD) is in the range of 20%~90%. Table 4.1 also shows the assumed homogeneous initial SOCs of both electrodes. Figure 4.1 depicts a fully charged SOC distribution for each electrode along the thickness of a battery; this is obtained by charging a battery for 3400 seconds.

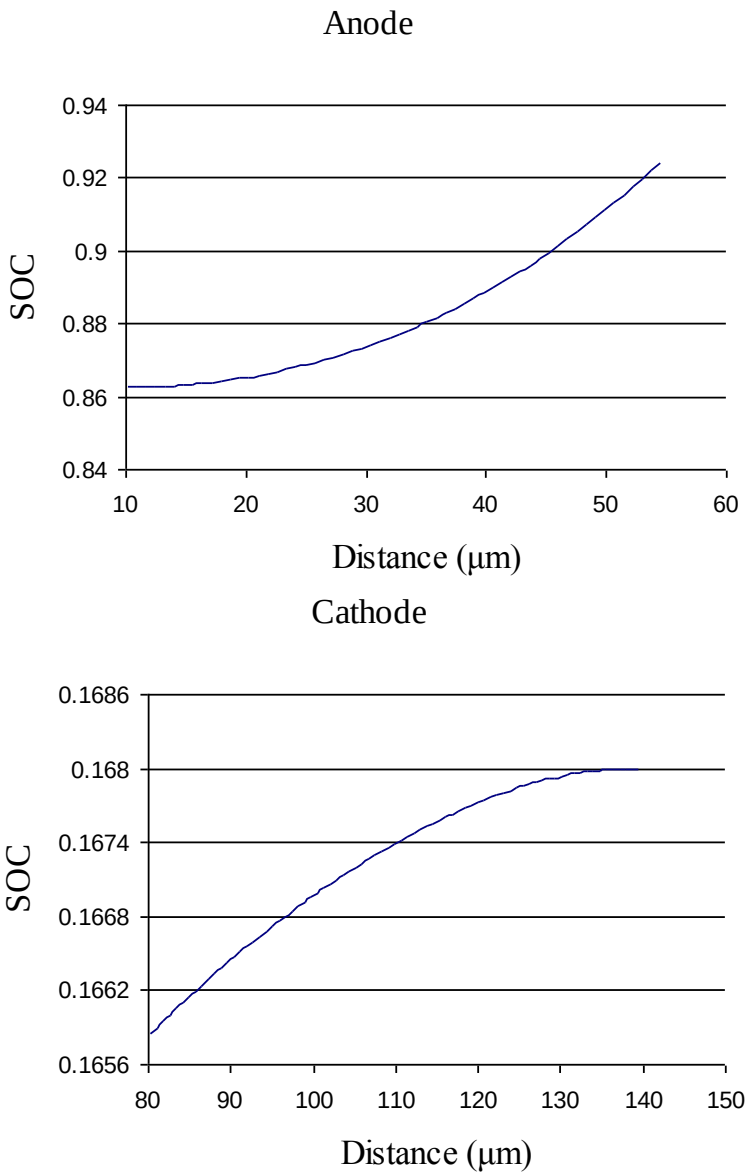

Figure 4.1 Final SOC of both anode and cathode

4.2 Effective Length

A pouch cell has a large length to thickness ratio. Therefore it is not feasible to build a finite element model with the actual dimensions of each individual component layer for the entire battery cell. To solve this problem, the influences of length on the local strain and stress distribution of the separator are studied.

In this work, a group of models with different lengths are developed. The results show that the maximum strain always emerges at the end of a charging period, and is located in the inner surface of the separator where it wraps around the corner of the anode. Figure 4.2 presents the strain contours obtained around a corner. Here strain is plotted in the x and y directions, and the corresponding maximum values are found along the horizontal and vertical segments of the separator near the edge. When plotted in the 1^{st} principle strain, the maximum value of the separator is found at the area in contact with the corner of the anode. As shown, the contour of the 1^{st} principle strain of the separator around a corner follows the shape of the corner.

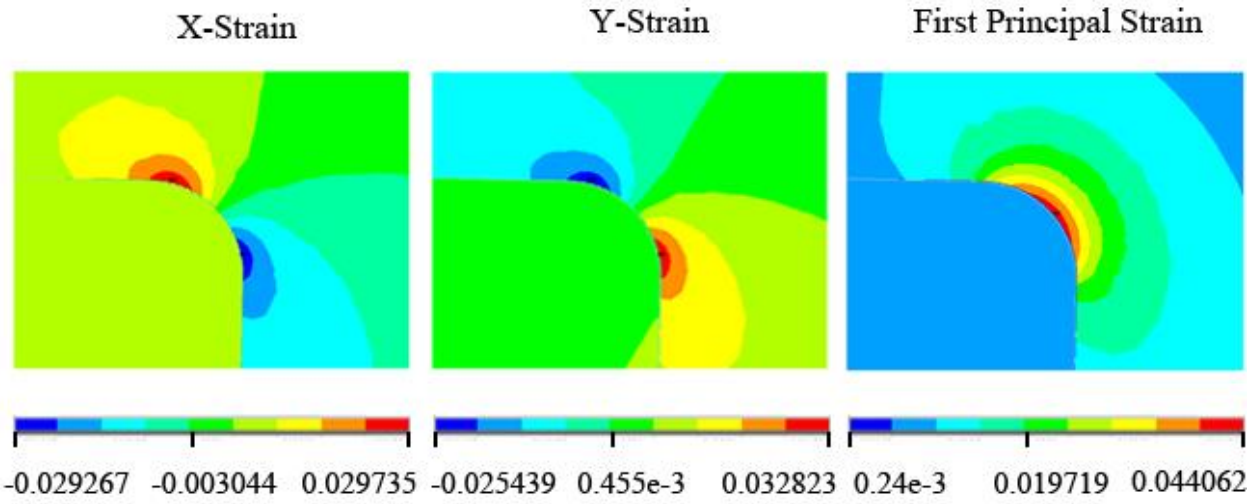

Figure 4.2 Contours of strain components near the corner

Figure 4.3 presents the maximum values of the strain components versus the model's length. As shown, the variation trends for all the components are generally the same: firstly strains decrease with increasing model length and then approach stable values when the length is larger than 4 mm. For this research, a length larger than 4 mm is deemed to be an effective length. Correspondingly this model could represent the whole battery cell.

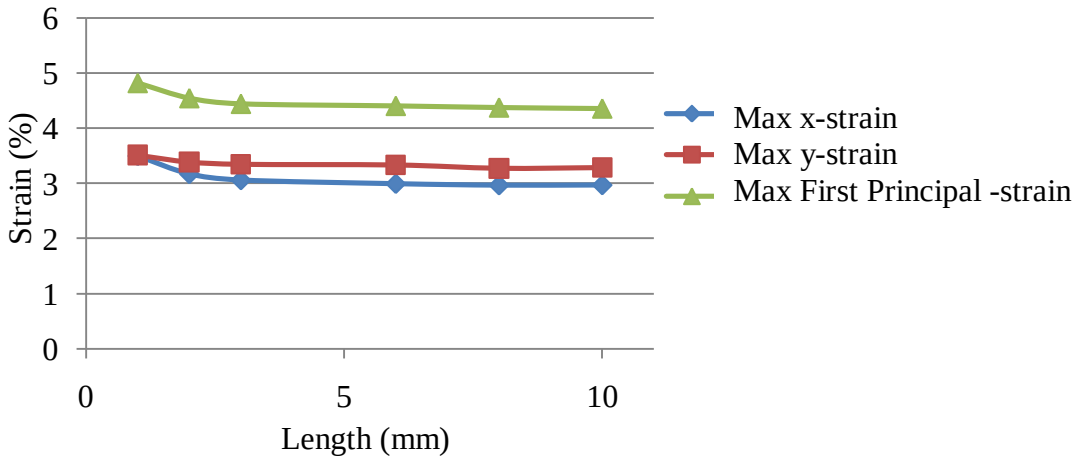

Figure 4.3 Strain components versus model length

Figure 4.4 presents a real scale 2-D model. The length of this model is 7 mm (>4mm).

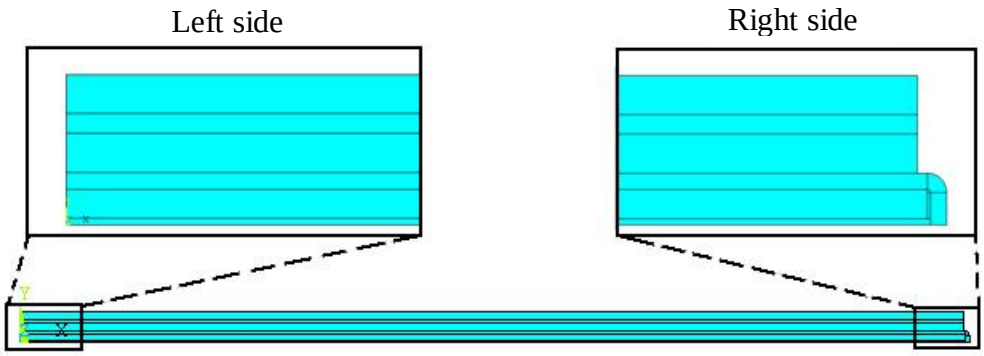

Figure 4.4 Macro scale 2-D model in ANSYS

4.3 Thermal Effect

For a battery in operation, temperature rise is an inevitable phenomenon. As mentioned in Chapter 1, thermal stress resulted from non-uniform thermal expansion can greatly change the stress conditions of the separator. To better understand the stress conditions of a separator in operation, self-heating of the battery must be considered. In this research, the thermal effect is studied by comparing the stress conditions of the separator in the models with and without temperature change.

4.3.1 Temperature Change

The temperature problem is solved with a full cell model in COMSOL. After running under exactly the same electrochemical conditions for the same amount of time (3400s), the temperature distribution of the whole battery is obtained. As shown in Fig. 4.5, the temperature near the convective boundary is relatively low due to the direct convection with air. However, the gradient of temperature is very small over the whole field, with an overall temperature change of less than 0.006 (from 336.76 K to 336.766 K). This is because the lithium-ion battery cell is very thin and most battery components are good thermal conductors. The temperature can be treated as independent of position (homogeneous at any given time) [31].

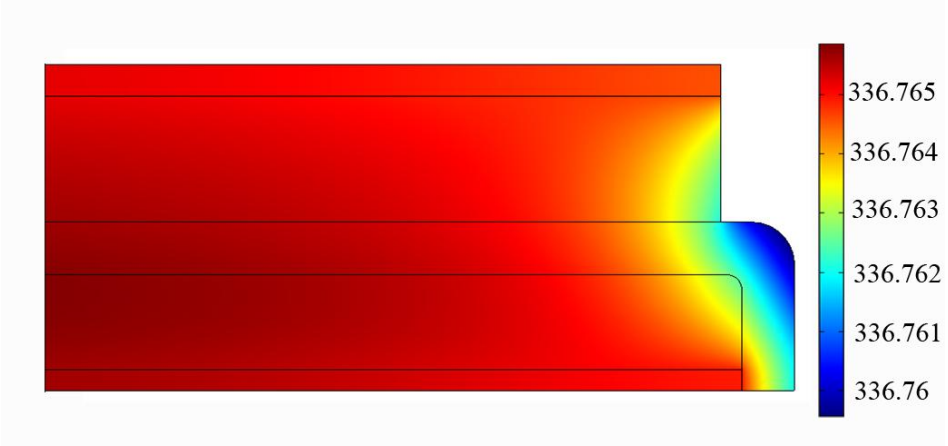

Figure 4.5 Temperature distribution of the whole battery

In reality, a thermal management system is always designed as part of a battery to control the temperature. This system is not just used to remove the heat generated inside the cells, but also the heat from resistive circuit elements around the cells. It is rather complicated to add this thermal management system into the simulation model in this research. However, since the best operation temperature is always maintained between -10 ℃ and 52 ℃, a uniform temperature can

be assumed within this range. In this study, the homogeneous temperature change is assumed to be 38.8 K (within the best operation temperature range) during one charging period.

4.3.2 Thermal Effect

The thermal influence on separators is investigated by comparing the simulation results of the models with and without temperature change. Figure 4.6 compares the x-displacement field for the two cases. As expected, with thermal effects, the total x-displacement of all battery components increases as a result of both mass diffusion expansion and thermal expansion. The corresponding average x-strain of the separator increases from 0.729% to 0.806%.

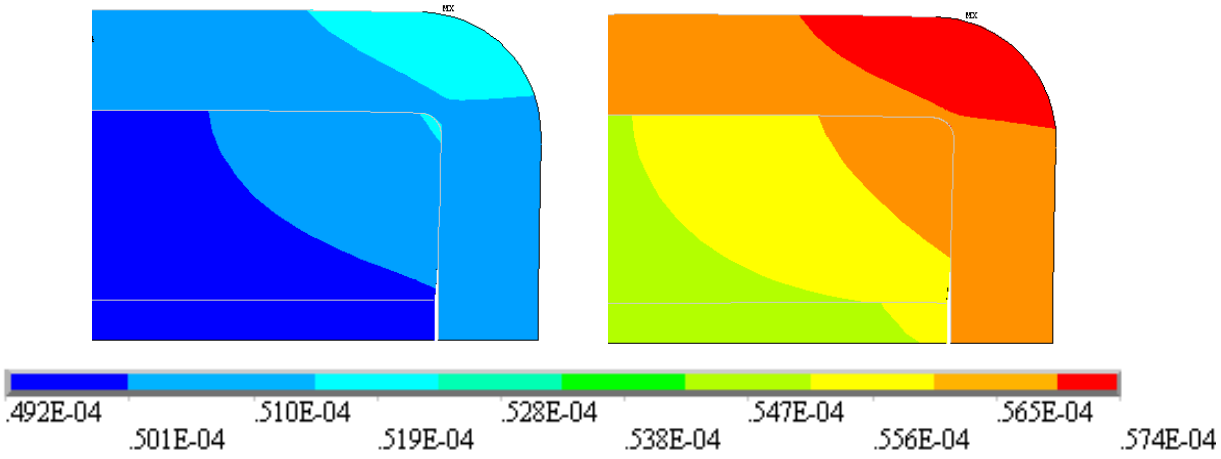

a) Without thermal effect b) With thermal effect

Figure 4.6 X-displacement of the battery model

Figure 4.7 compares the Von Mises stress field for the two cases. As shown, in both conditions, the maximum Von Mises stress occurs at the center of the inner surface of the separator, which is the area in contact with the corner of the anode. This study also shows the stress in the separator

decreases dramatically after introducing thermal effects into the model. The maximum Von Mises stress changes from 27.2 MPa to 15.5 MPa, which represents about a 43% decrease.

This phenomenon can be explained by the types of expansion and the differential in thermal expansions among the battery components. In simulations without thermal effects, all deformations of the separator are driven by the outer source, like the deformation of the electrodes induced by lithium ion diffusion. With thermal effects, a part of the deformation in the separator is contributed by thermal expansion (eigenstrain), and this deformation is much greater than that of the other components of the battery because the thermal expansion coefficient of the separator is much larger. Meanwhile, since the total strain of the separator and the anode would remain the same, an increased eigenstrain would decrease lithium diffusion induced strain. Overall, the much larger value of the thermal expansion coefficient of separator reduces the local strain of the separator dramatically.

Figure 4.8 compares the 1^{st} principle stress field for the two cases. The distribution of the 1^{st} principle stress in the separator near the corner of the anode is very similar to that of the Von Mises stress. For the models with and without thermal effects, the maximum 1^{st} principle stresses are 10.9 MPa and 17.8 MPa, respectively. The contour of the 1^{st} principle stress in this area follows the shape of this corner.

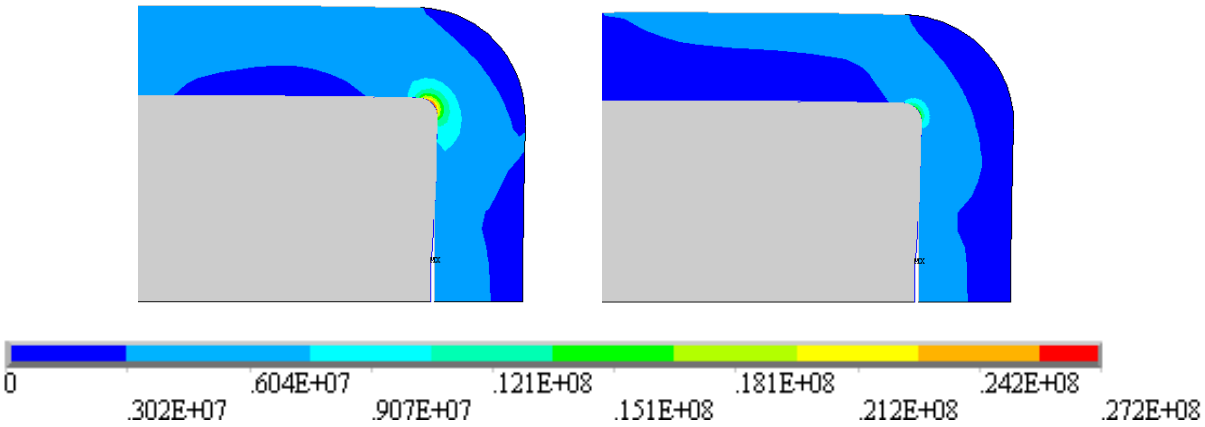

a) Without thermal effect b) With thermal effect

Figure 4.7 Von Mises stress of the battery model

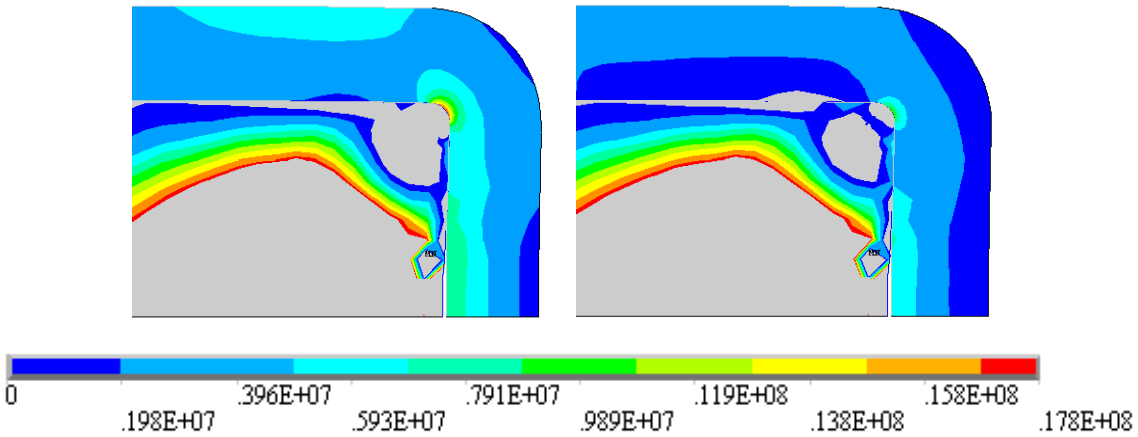

a) Without thermal effect b) With thermal effect

Figure 4.8 1st principle stress of the battery

Table 4.2 Comparisons of the models with and without thermal effect

	Average x-strain (%)	Average y-strain (%)	Maximum Von mises stress (MPa)	Maximum 1st Principal stress (MPa)
Without thermal effect	0.729	-0.40	27.2	17.8
With thermal effect	0.806	0.20	15.5	10.9

Above all, the comparisons of the models with and without thermal effects are listed in Table 4.2. As presented, there would be a huge difference between the models with and without thermal effects. To better approach the real working conditions of a battery, thermal effects in all the simulation models will be considered in the following studies.

4.4 Model Validation

This study is sponsored by General Motors (GM). The model prediction is in reasonable agreement with the experiments conducted at GM. The data will be released in a later time.

4.5 Results and Discussion

Lithium ion batteries all undergo a similar production process; however, there is variation between batteries due to material selection and the shape of the battery components. Based on the literature studies [13, 16, 23], a series of parameters were found to have a potential effect on the strain & stress conditions of a separator. Some of these parameters include the porosity, interactive forces between separator and electrodes, pressure on the upper surface, thickness of the separator, particle sizes of the electrodes. They can be generally classified into three groups: external factors, internal factors and manufacturing factors as shown in Table 4.3.

Table 4.3 Categories of potential factors

	External factors	Internal Factors (for electrodes)	Manufacturing Factors
Factors	Friction Pressure Temperature	Particle radius Porosity Diffusivity	Thickness Multiple separators Corner shape

In this work, each category of factors is investigated independently. With the aid of the model discussed above, each of these factors will be optimized to form a more ideal battery design.

4.5.1 Friction

As introduced in Chapter 3, during the production process of a lithium ion battery, both electrodes firstly attached to a collector and then come in contact with either side of the separator. These contacts may result in friction and viscous resistance between the components. In the simulation model, contact is defined between the separator and adjacent electrodes. A corresponding effective friction is introduced for each pair of components in contact.

The effective frictions are used to simulate the effects of all kinds of interactions. Since the separator is relatively soft, the influence of the interactions between the separator and the electrodes can be significant. Without changing other conditions, the study of the effective friction is transferred to the study of the effective friction coefficient between these surfaces. In this work, simulation was conducted with different effective friction coefficients ranging from 0.0 to 0.4. Also the effective friction coefficient between the separator and the anode is assumed to be the same with that between the separator and the cathode.

As shown in Figure 4.9, the influence of friction can be significant. Generally an increased effective friction coefficient results in a greater maximum stress evaluated by both Von Mises stress and the 1^{st} principal stress. This can be explained by the fact that in order to generate a

certain deformation, the separator needs to overcome the resistance coming from it and the surrounding components. Since the resistance from the surrounding components increases with friction, to generate the same amount of overall deformation, the local deformation of the separator (where friction occurs) will also increase to counteract it.

The friction coefficient does not only affect the magnitude, but also the position of the maximum stress. Figure 4.10 demonstrates this effect; as the value of the friction coefficient causes the maximum stress to increase, its location in the separator gradually shifts from the center of the corner to the upper part of the corner. This phenomenon can be explained by the fact that the anode has a much larger contact surface with the upper side than the right side of the separator. This large ratio results in the friction affected stress concentrating on the upper part of the separator. It is also the reason why the stress values obtained by the numerical experiment fluctuate around the trend lines in Figure 4.9.

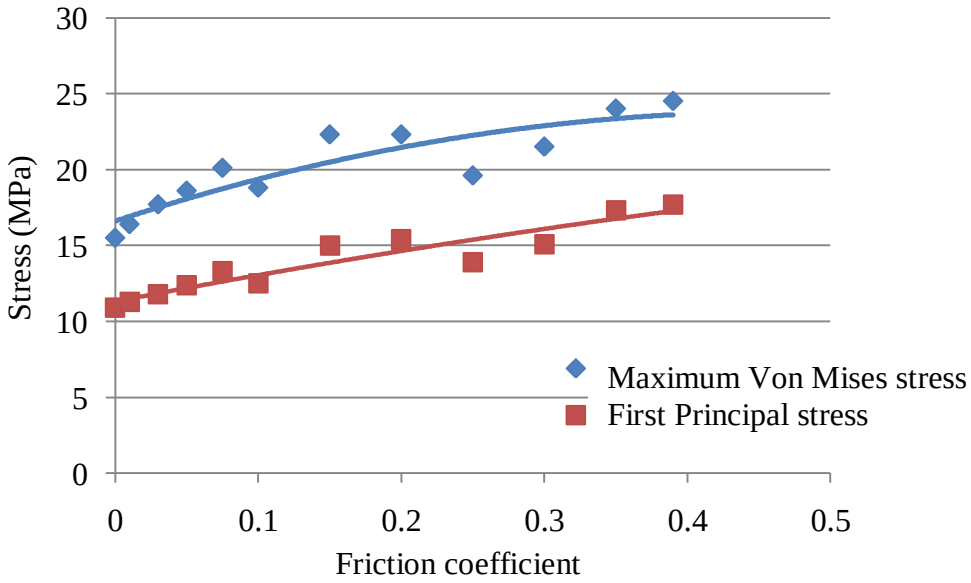

Figure 4.9 Stresses versus friction coefficient

In the numerical study shown in Figure 4.11, it has been found that homogeneous stress fields are always formed in the majority of the separator, which is far away from its right side boundary. By introducing friction, the Von Mises stress value of this area slightly drops from 2.71MPa to 2.62MPa, but variation of the friction coefficient doesn't affect the Von Mises stress. Figure 4.12 presents the Von Mises stress of this stable area of the separator versus different friction coefficients.

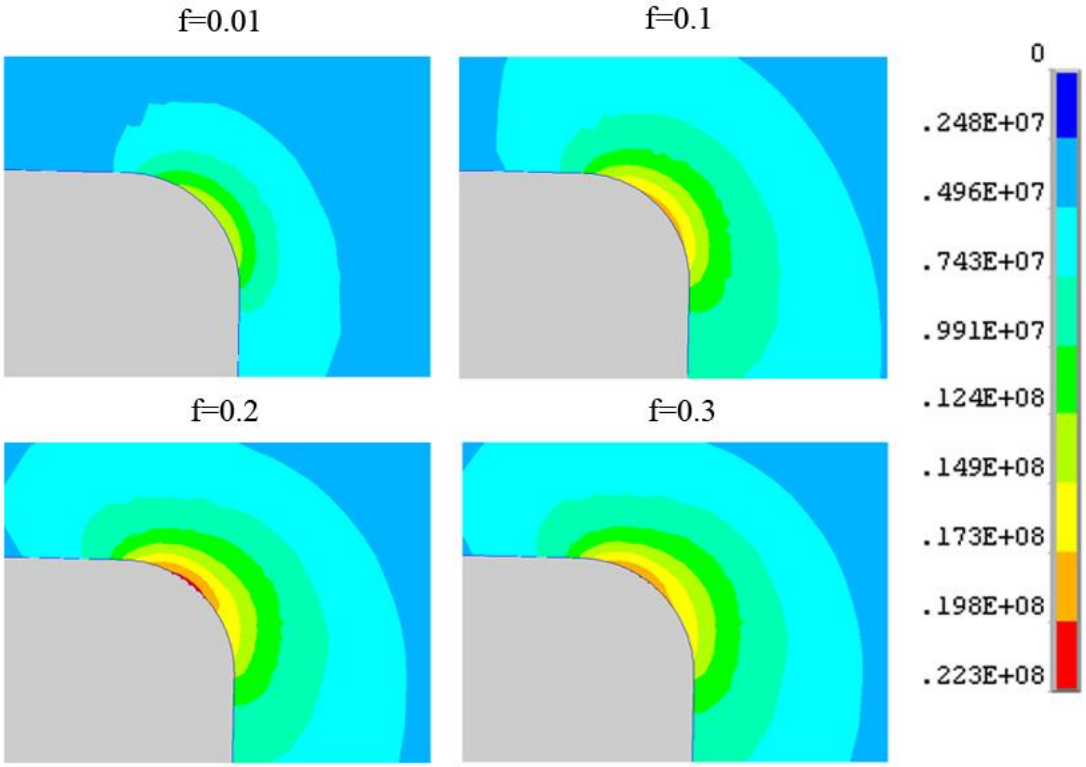

Figure 4.10 Von Mises stress in the corner under different friction coefficient conditions

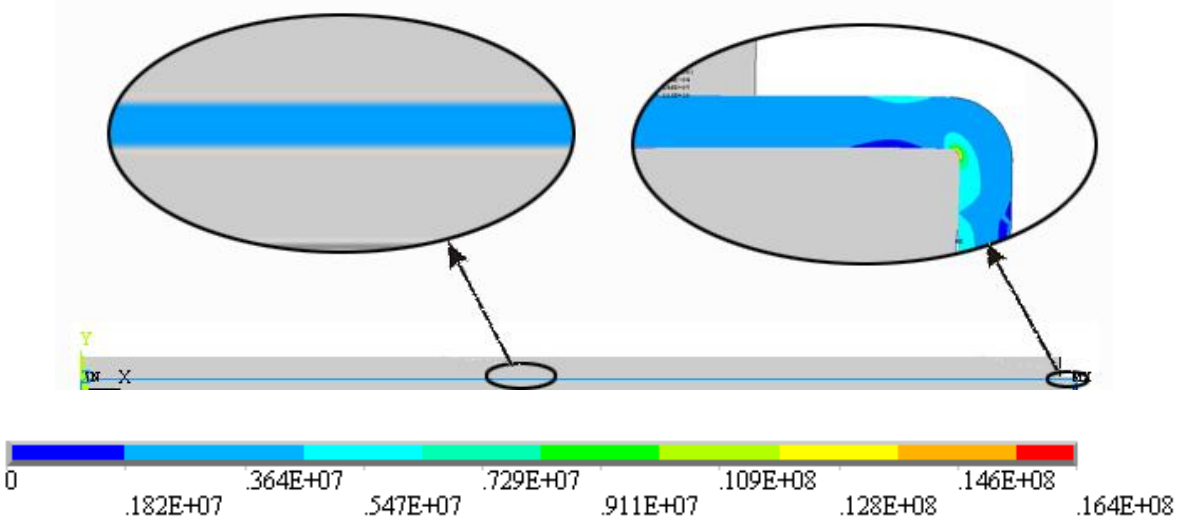

Figure 4.11 Von Mises stress of the separator

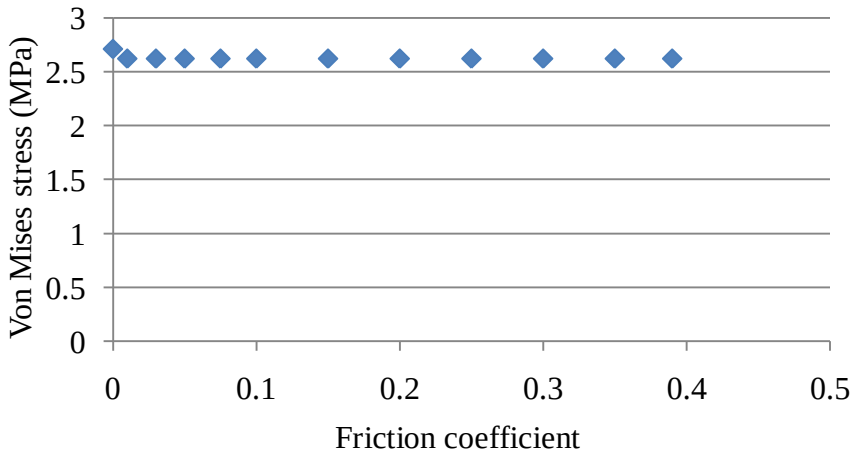

Figure 4.12 Von Mises stress of the stable area of the separator

From the above results, it can be concluded that friction can only affect the side part of the separator by shifting the location of the maximum stress and increasing its value. Generally, better stress conditions in a separator could be achieved by reducing or softening the interactions

between the separator and its surrounding electrodes. This can be treated as a reference standard when choosing materials for the components of lithium ion batteries.

4.5.2 Pressure

In this study, the prismatic pouch cells have a flexible, foil-type case. In applications, to maintain the volume, the battery packs are clamped between a pair of parallel plates, which is equivalent to applying a uniform pressure at the surface of a pouch cell. Pressure could affect the contact conditions between different components, the overall electrochemical performance, as well as the mechanical performance. In this research, only the influence of pressure on the mechanical performance of the separator is studied. Considering the pressure could also change the friction between the separator and its surrounding electrodes, all friction coefficients are assumed to be zero in order to study the effects of pressure independently.

The pressure range considered in this study is 5psi ~ 90psi (0.0345MPa~0.621MPa). Figure 4.13a shows the influence of pressure on the average strain components. As presented, the x component of the average strain increases with pressure, while the y component decreases with pressure. The increment of the x component is relatively small compare to the decrement of the y component. This is because the pressure is only added in the y direction and the dimension in the x direction is much larger than that in the y direction, therefore the separator deforms more easily in the y direction. The y component decreases with pressure because the thermally induced eigenstrain is a positive value, thus lower average strain yields a larger deformation.

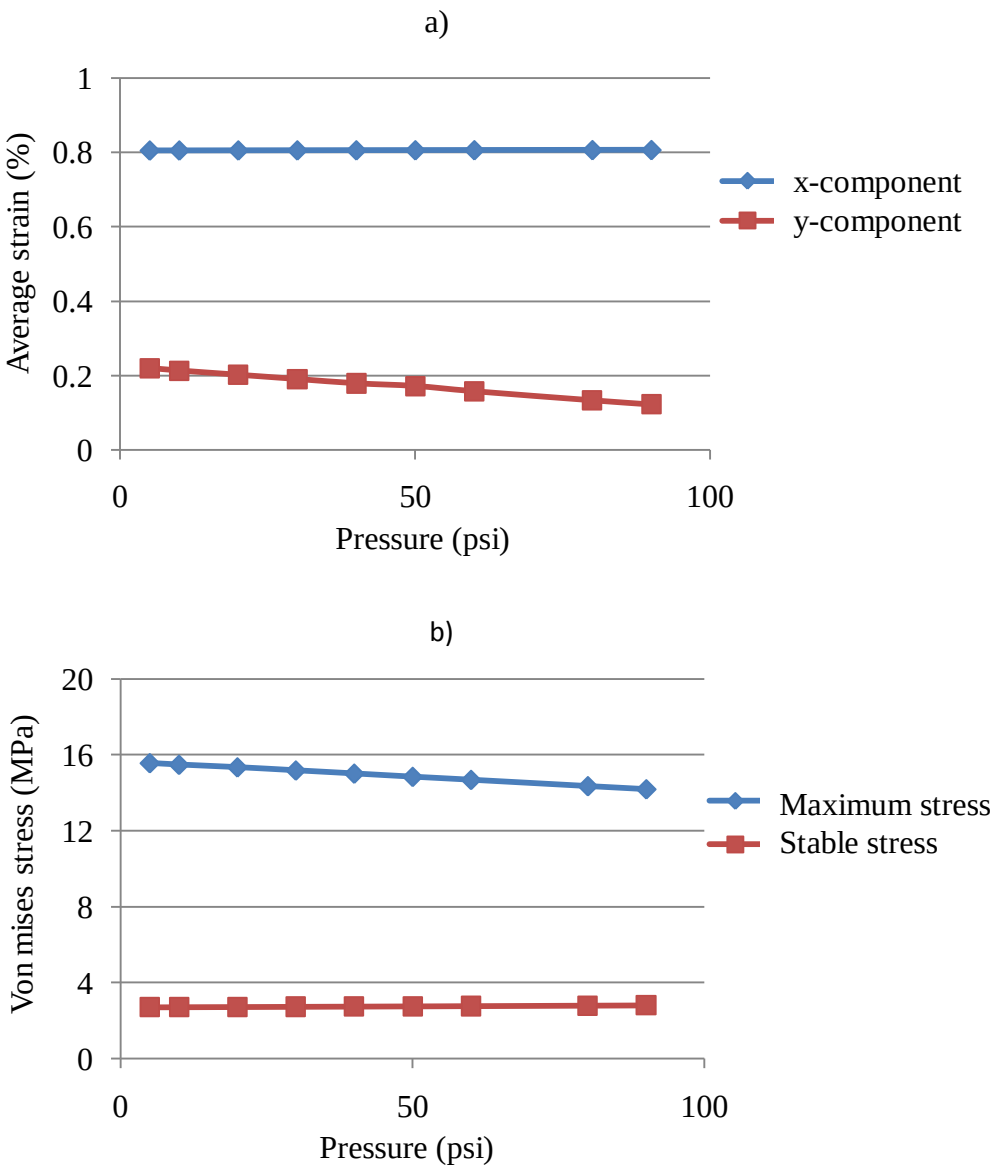

Figure 4.13 Effect of pressure on (a) the average strain components, (b) the Von Mises stress of the separator.

Figure 4.13b shows how pressure influences the stress conditions on the separator. This chart indicates that increasing pressure causes the maximum Von Mises stress to decrease and the stable Von Mises stress on the left side of the separator to increase. The former effect can be explained by the fact that higher pressure increases the deformation of the separator in x direction; which, in order to maintain volume, decreases the anode expansion induced

deformation at the same time. The latter effect is consistent with the change of the y component of local strain as illustrated above. The change of the stable Von Mises stress is very small. It can be treated as independent of pressure in the range of 5psi~90psi.

Unlike the friction, pressure does not affect the position of the maximum stress, which, as shown in Figure 4.14, is always located in the inner surface near the corner of the anode. It's important to note that in the upper surface of the separator near the corner of the cathode, a high stress area gradually forms with increasing pressure. In this area the effect of the pressure is evident. Both stress level and its area expand with increasing pressure.

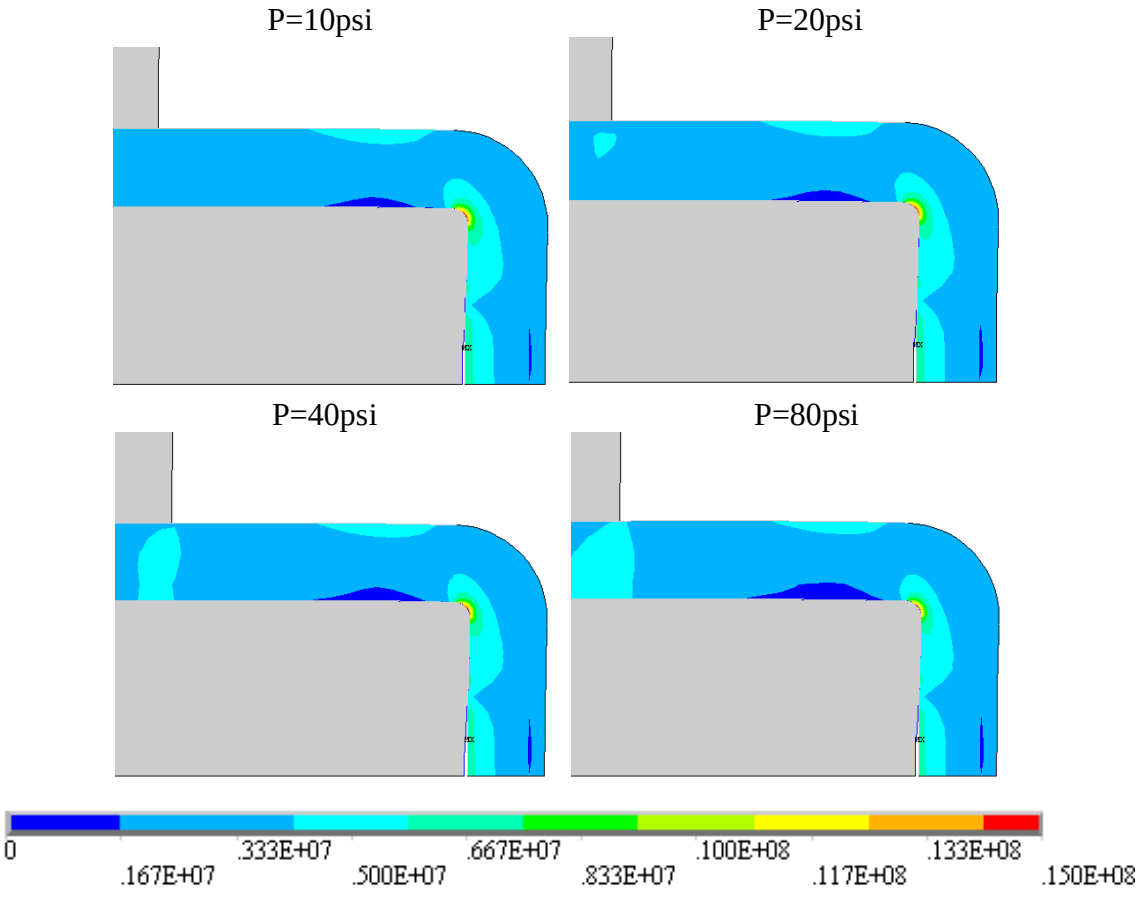

Figure 4.14 Von Mises stress condition of the separator under different pressures

In summary, since higher pressure results in a lower maximum stress and unchanged stable stress in the separator, the mechanical performance of the separator can be improved by introducing higher pressure. However, in a general working condition, when the pressure just ranges from 5psi to 20psi; its influence over stress conditions in the separator is very small (within 1.5%, predicted by this model).

4.5.3 Combination of Friction and Pressure

As discussed in 4.5.2, pressure is able to affect the stress conditions of the separator by changing the deformation of the separator directly and friction between the separator and electrodes. Therefore, when designing a battery, it is important to consider both friction and pressure. In this study, both factors are explored in order to optimize the best external operating conditions on the separator.

As shown in Fig. 4.15a and 4.15b, the scatters of both the x- and y- components of the average strain overlap under different friction coefficients. In Fig. 4.15a, the x component of the average strain remains constant under all friction and pressure conditions, which indicates the overall deformation of the separator in the x direction is independent of both friction and pressure. In Fig. 4.15b, the y component of average strain decreases linearly with increasing pressure regardless of the friction coefficient. This is inconsistent with the results obtained in 4.5.1 and 4.5.2. Overall, it can be concluded that friction cannot effect the overall deformation of the separator, and pressure can only produce some effect in the y direction.

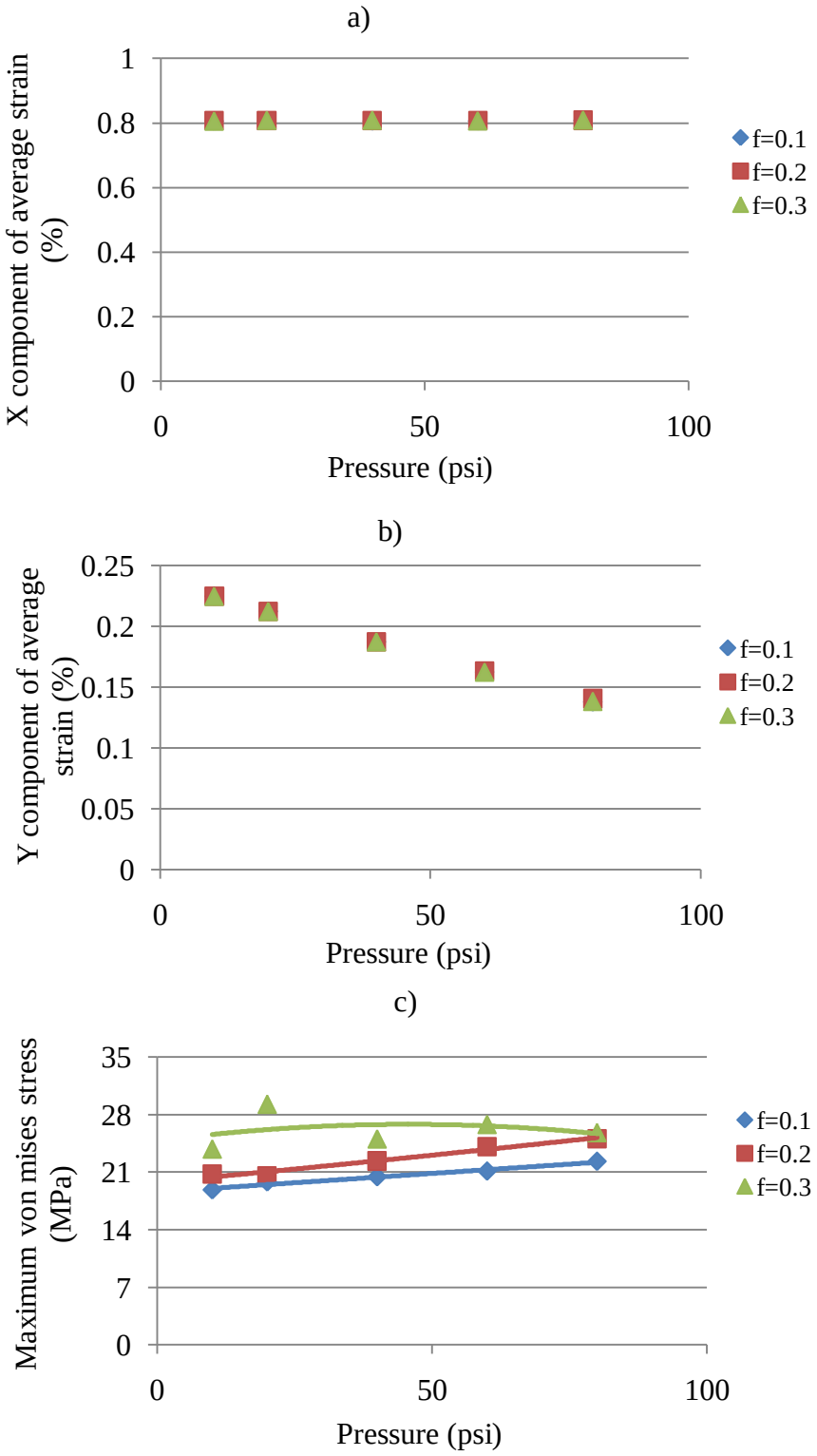

Figure 4.15 Influences of both pressure and friction on the strain & stress conditions of the separator

However, the influences of both factors on local strain are significant as presented in Figure 4.15c. Generally, higher friction coefficients can result in larger maximum Von Mises stress. When the friction coefficient is small (≤ 0.2), the maximum Von Mises stress increases with pressure. When the friction coefficient is relatively large, such as 0.3, the maximum Von Mises stress fluctuates around a certain value.

For a general operating pressure of less than 20psi, and a friction coefficient less than 0.2, the value of the maximum Von Mises stress stays in a relatively small range. This condition can be recognized as the best external operation conditions for the separator.

4.5.4 Temperature

Battery temperatures are capable of affecting the battery's performance and life. As mentioned in 4.3, the thermal management of the battery is a critical element for achieving the desired performance and calendar life for the battery; for this reason researchers are paying increasing attention to battery thermal analysis and management. For the linear system considered in this study, thermal effect is only represented by thermal expansion, which is a result of temperature change. Since the best operating temperature is always maintained in the range of -10 ℃~ 52 ℃, uniform temperature change is assumed to range between 10K and 60K.

As presented in Fig. 4.16, the maximum Von Mises stress decreases linearly with increasing temperature change. This value can drop dramatically from 24MPa to 9.6MPa as shown in Fig. 4.17. This phenomenon can also be explained by the differential in thermal expansions of the

battery components. The relatively large thermal expansion coefficient of the separator can further reduce the local strain of the separator under larger temperature change by introducing more thermal eigenstrains.

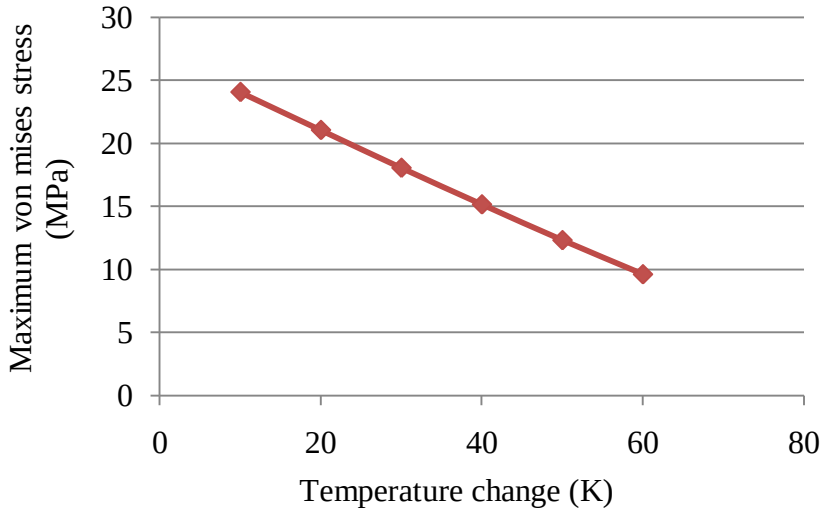

Figure 4.16 Maximum Von Mises stress of the separator versus temperature change

Figure 4.17 shows the position of the maximum Von Mises stress gradually shifts from the center to the lower side of the corner of the separator.

In conclusion, higher temperature change results in a lower maximum stress in the separator, lowering the possibility of failure. However, it should be noted that higher temperatures can affect the electrochemical performance of a lithium ion battery, or even cause safety problems. Therefore temperature change should be managed properly. The assumed temperature change (38.76K) in this study is a reasonable value.

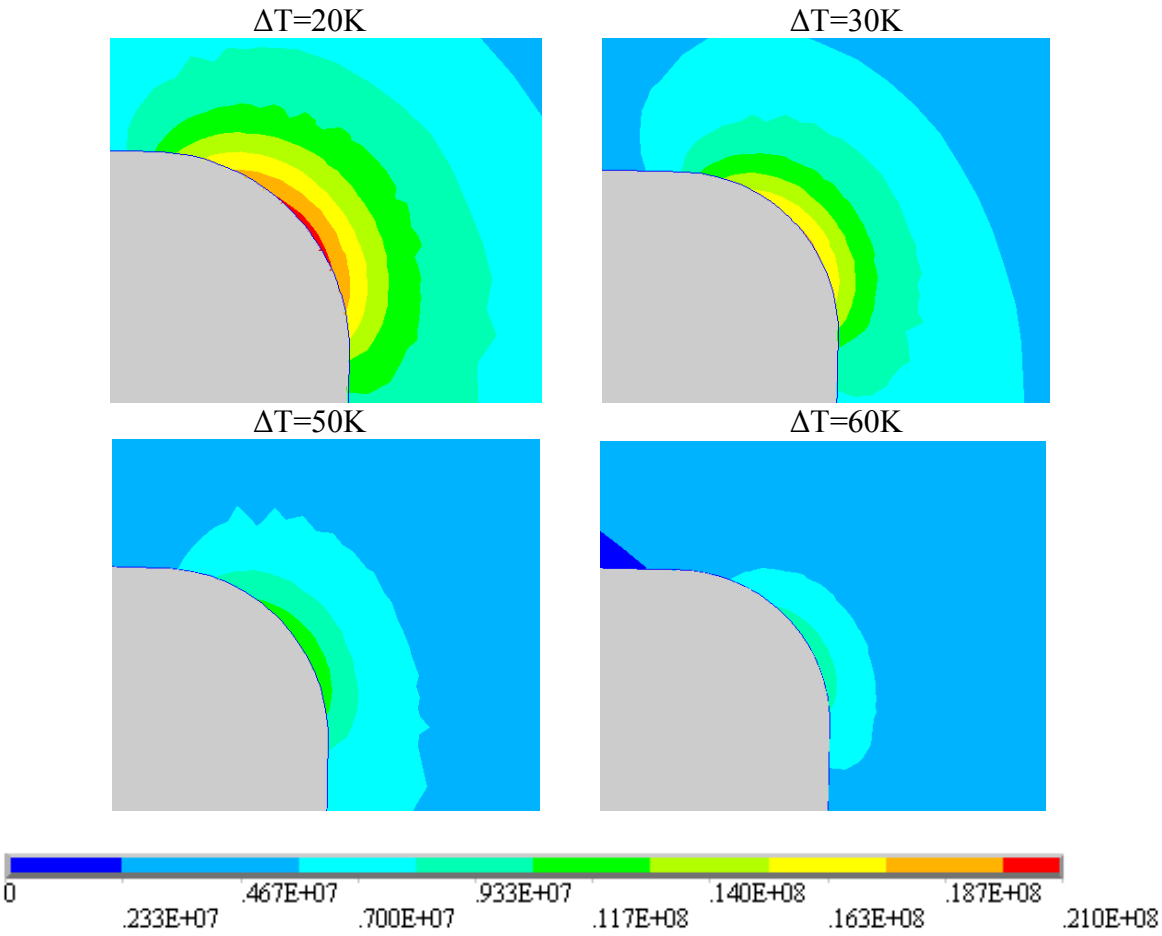

Figure 4.17 Von Mises stress condition of the separator around the corner

4.5.5 Particle Radius

Particle radius is an important factor that researchers are interested in. Researchers have shown that smaller particle radii can result in smaller lithium gradient induced hydrostatic stresses inside the electrode [16, 23]. However, the influence of particle radii on the overall deformation of the electrode and the separator is not known.

In this part of study, three pairs of particle radii of the anode and cathode are used to perform the analysis. They are estimated from Reference 34 and Reference 35 by using the values of the r10, r50 and r90 particle radii, as shown in Table 4.4.

Table 4.4 Three pairs of particle radius

	Pair1 (r10) (μm)	Pair2 (r50) (μm)	Pair3 (r90) (μm)
Anode	8.4	11.5	16
Cathode	2.45	3.35	4.65

*The definition of r10 is: the equivalent radius that 10 % particles of the electrode have a smaller equivalent radius than this value [43]. The definition of r50 and r90 can be derived similarly.

In this study, the particle radius is changed under the same volume fraction of active materials for both electrodes. Figure 4.18 presents the lithium concentration of both the anode and cathode along the thickness at the end of a charging period with different particle radii.

As shown, the particle radius can change the average cross-section lithium concentration. For the anode, higher anodic particle radii result in a smaller lithium concentration gradient, while the cathodic particle radii can only change the absolute value of the concentration. For the cathode, higher cathodic particle radii result in a larger concentration gradient, while the anodic particle radii can nonlinearly change the absolute value of the concentration.

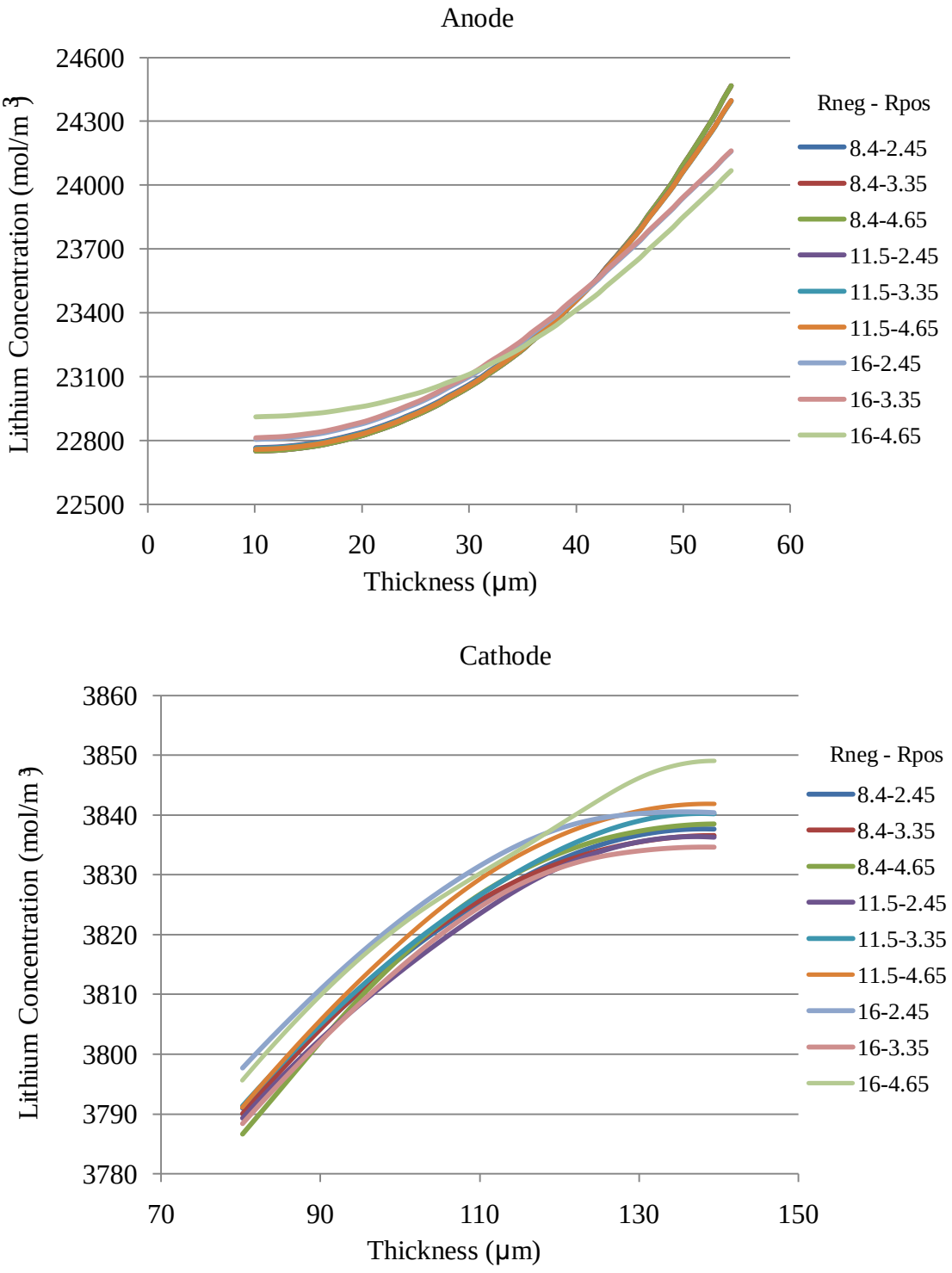

Figure 4.18 Concentration distributions along the thickness of the electrodes

Figure 4.19 presents the maximum Von Mises stress of the separator under differing particle radii. As shown, the maximum Von Mises stress is maintained around 15.5MPa regardless of the particle radii. This can be explained by the fact that even though the lithium concentration along the thickness is changed by the particle radii, the overall changes in both electrodes are very small. Taking the anode as an example, high particle radii, like 16-4.65μm, can increase the concentration in lower thickness area up to 1.2%, but it can also decrease the concentration in higher thickness area by the same percentage. Therefore, the average concentration in the whole anode changes very slightly.

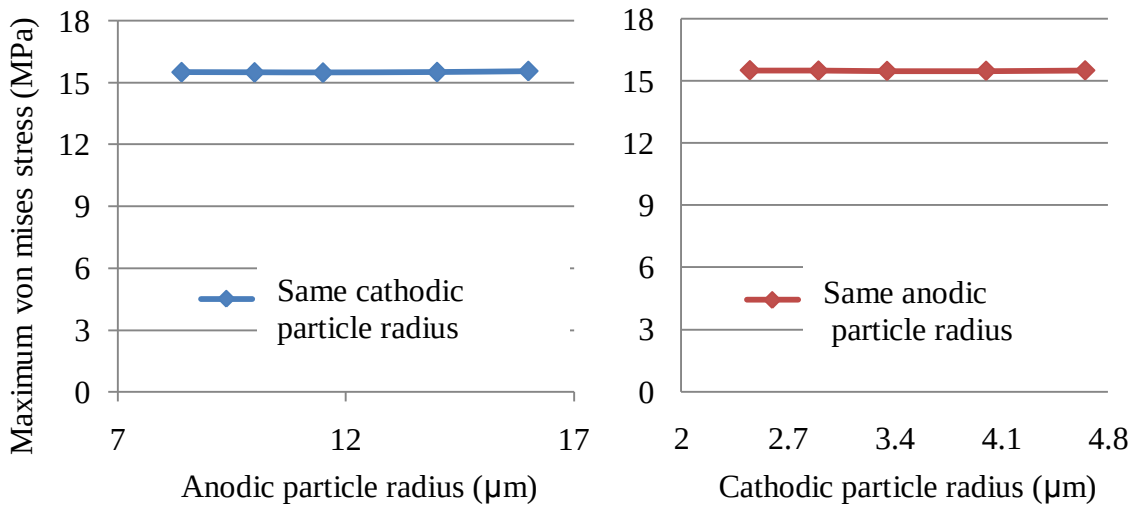

Figure 4.19 Maximum Von Mises stress of the separator under the conditions with different particle radii

In conclusion, under the same volume fraction of active materials for both electrodes and the same temperature change, the particle radii do not yield any effect on the maximum stress of the separator. However, in reality smaller particles are often preferred due to some other

performances, like particles with smaller size may deliver more power, energy, and decrease the lithium gradients induced hydrostatic stresses inside the particles of active materials. [16, 23]

4.5.6 Thickness of Separator

For high energy density applications, smaller separator thickness is desirable in order to achieve a lower internal resistance. However, the safety concern with respect to mechanical integrity and penetration must be considered. The thicker the separator, the greater the mechanical strength and the lower the probability of punctures during cell assembly, but the larger the overall volume of the whole battery. In recent years, a trend to achieve higher capacity is by reducing the thickness of the separators [8], which gives more space for active materials. The most widely used thickness for the separator of lithium ion batteries ranges from 20μm to 30μm.

As shown in Fig. 4.20, in the range of 20μm to 30μm, the maximum Von Mises stress in the separator increases with increasing thickness as the stress in the stable parts of the separator slightly decreases. This indicates that a thinner separator sustains a relatively small maximum stress during cell operation.

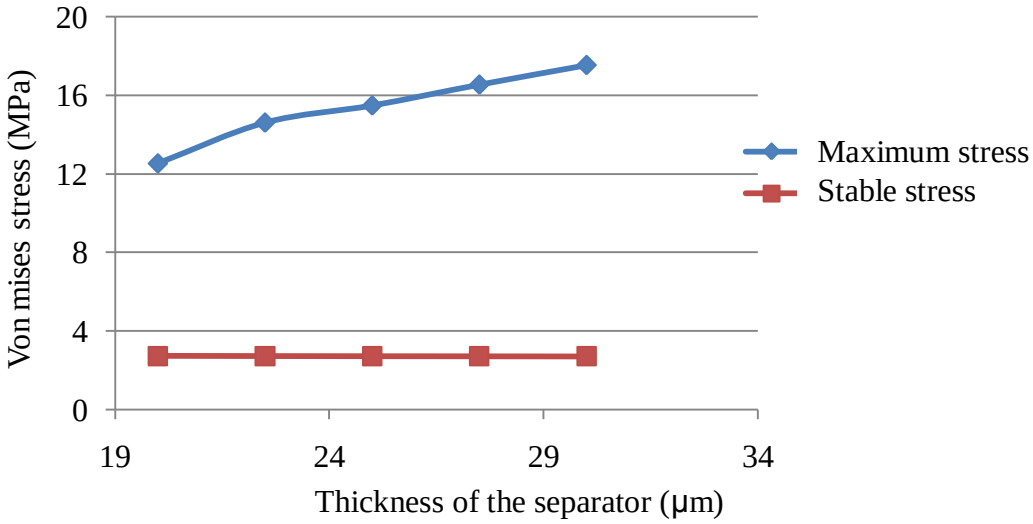

Figure 4.20 Von Mises stress of the separator versus thickness

In conclusion, thinner separators can result in smaller maximum stresses in the separator in operation. However, it should be noted that shorter thickness could also bring in lower mechanical strength and higher probability of punctures during cell assembly.

CHAPTER 5 SUMMARY AND CONCLUSION

5.1 Summary and Conclusion

In this research, a numerical model for the stress analysis of separator in a prismatic lithium ion battery is developed. Three groups of phenomena that occurred inside the battery cell were considered in order to perform the stress analysis. They are electrochemical, thermal and mechanical phenomena. The two main sources of stress on a separator investigated in this study are lithium diffusion induced and thermally induced stress.

By introducing self-heating phenomena and a modified strain relationship into the pseudo 2-D models proposed by Doyle et al., a macro-scale 2-D 1.5-cell model was developed to evaluate stresses in the separator of a pouch cell. In this model, the electrodes and the separator were treated as homogenized media. The porous electrodes were considered a composite of electrode particles in an electrolyte matrix, and their effective properties were computed using the rule of mixtures. To couple these two models, this study also introduced two other connecting models. The simulation processes were divided into two steps: obtain the lithium and temperature distributions in COMSOL, and then perform stress analysis in ANSYS. The mechanical influences of stress on the lithium and temperature distributions were neglected. This approximation was discussed in Chapter 4.

It was demonstrated that the maximum Von Mises stress of the separator always emerged at the inner center of its corner when the lithium ion battery was fully charged, and the rest of the separator was in a relatively low and stable stress state. This study focused on this area vulnerable of failure.

A verified effective length was used in this study to solve the infeasibility of building an entire battery due to its large length to thickness ratio.

Thermal effects were demonstrated to be significant. The simulations revealed that although the thermal expansion increased the average strains in the electrodes and in the separator, the local maximum stress and strain in the separator actually decreased with rising temperature.

External, internal and manufacturing factors were studied with a 2-D battery cell model at the same fully charged state. It was shown that the maximum Von Mises stress increased with increasing separator thickness and interactions between the separator and its adjacent electrodes, while the stress decreased with increasing surface pressure and temperature change of the battery. Under the same volume fractions of active materials, the particle radii of both electrodes didn't affect the stress conditions in the separator. Thus, the optimized conditions for these factors are: low effective friction coefficient (<0.2), high pressure, large temperature change and thin thickness. However, it should be noted that in reality some additional performances of a battery should be considered when optimizing these parameters. For example, thinner thickness can result in lower mechanical strength and a higher probability of punctures during cell assembly, and the temperature cannot exceed the best operating temperature range.

In summary, the simulation models made in this study can be used as a design tool to optimize the stress conditions in separators. The predicted results can work as reference conditions for the design of lithium ion batteries.

5.2 Future Work

This is the first reported work on stress analysis of a separator inside a lithium ion battery. Limited by the knowledge on the multi-physics problems and database, linear and homogeneous assumptions were made in the model, thus the stress values derived from this model are not accurate. However, this model can be used to analyze the general stress conditions of the separator in a lithium ion battery cell and the trend of the influence of some design adjustable parameters. In order to advance this study, further work is need in the following two aspects: (1) improvement of the existing model, and (2) fundamental studies on material constitutive behaviors.

5.2.1 Improvement of the Model

The accuracy of the simulation models and the coupling methods may be improved. The areas to be improved include:

1) Develop a realistic porous material model to replace the homogeneous solid models.
2) Consider the shape of micro-scale particles around the area of potential failure.

3) Improve the robustness of the contact definition in COMSOL so that all the phenomena may be simulated simultaneously.
4) Consider the effect of stress on diffusion.

With an improved model, in addition to revisiting the parameters investigated in this thesis, further investigations may be conducted to study the prismatic cells with alternative methods of wrapping and to study the stress in cylindrical cells.

5.2.2 Fundamental Studies on Material Constitutive Behaviors

In order to better approximate real world conditions, nonlinear relationships should be considered instead of linear assumptions. In a parallel project, the viscoelastic behavior of polymeric separator in battery environment and its modeling is under investigation [46]. In future work, a time, temperature dependent constitutive model for separator can be incorporated into the model developed in this work.

Recent studies revealed that, with increasing lithium concentration, the Young's modulus of the anode materials can change up to three folds. It was reported that Si–Li phase decreases [47] whereas the Young modulus of C-Li phase increases [48] with lithium concentration. Experimental investigations will be conducted to verify these computational results and concentration dependent constitutive models will be developed.

APPENDICES

APPENDIX A

The electrochemical boundary conditions for pseudo 2-D models are listed in Table A.1.

Table A.1 Electrochemical boundary conditions for pseudo 2-D models [10,13]

	1-D Porous Electrode Model				2-D Spherical Particle Model	
	1*	2	3	4	Upper surfaces	Other surfaces
Electronic current balance in the solid phase	$\varphi_1 = 0$	$n\nabla(-k_{1,eff}\nabla\varphi_1) = 0$		$n\nabla(-k_{1,eff}\nabla\varphi_1) = -i\_1C$ **	-	-
Ionic charge balance in the electrolyte	$n\nabla(-k_{2,eff}\nabla\varphi_2) = 0$				-	-
Mass balance in solid phase	-	-	-	-	$n\nabla(-D_1\nabla c_1) = \frac{i\_loc}{F}$	$n\nabla(-D_1\nabla c_1) = 0$

*1, 2, 3 and 4 are the four points in the 1-D porous electrode model.
**i_1C is the 1C charge current.

APPENDIX B

In this study, to have a robust contact definition between the separator and its adjacent electrodes, the macro-scale 2-D model is solved in ANSYS instead of COMSOL. Diffusion analysis is not available in ANSYS. Based on thermal-diffusion analogy, mass diffusion analysis can be performed using the thermal module. The correlation between mass diffusion and thermal diffusion is derived and depicted in this appendix.

B.1 Diffusion Equation

In AYSYS, the basis for thermal analysis is a heat balance equation obtained from the principle of conservation of energy [44], as shown in Equation B.1 in Cartesian co-ordinates. [45]

$$\rho c_p \left(\frac{\partial T}{\partial t} + V_x \frac{\partial T}{\partial x} + V_y \frac{\partial T}{\partial y} + V_z \frac{\partial T}{\partial z}\right) = \frac{\partial}{\partial x}\left(k_x \frac{\partial T}{\partial x}\right) + \frac{\partial}{\partial y}\left(k_y \frac{\partial T}{\partial y}\right) + \frac{\partial}{\partial z}\left(k_z \frac{\partial T}{\partial z}\right) + \ddot{q} \quad \text{(B.1)}$$

where, ρ is density, c_p is specific heat capacity, T is temperature, t is time, V is velocity, k is thermal conductivity, and $\ddot{q}$ is heat generation rate per unit volume. This is also the general form of the convection–diffusion equation. In this work, only diffusion is considered. The heat balance equation for the 2-D model can be simplified as:

$$\rho c_p \frac{\partial T}{\partial t} = \frac{\partial}{\partial x}\left(k_x \frac{\partial T}{\partial x}\right) + \frac{\partial}{\partial y}\left(k_y \frac{\partial T}{\partial y}\right) + \ddot{q} \quad \text{(B.2)}$$

While the concentration field induced by diffusion can be predicted by Fick's second law as presented in Equation B.3

$$\frac{\partial c}{\partial t} = \frac{\partial}{\partial x}(D_x \frac{\partial c}{\partial x}) + \frac{\partial}{\partial y}(D_y \frac{\partial c}{\partial y}) \tag{B.3}$$

where c is the concentration, D is the diffusion coefficient. Comparing Equation B.2 and B.3, $\ddot{q}$ is assumed to be zero since no mass is generated inside the lithium ion battery. In this work, the diffusion coefficient is also assumed to be isotropic. Therefore, Equation B.2 and B.3 can be simplified into Equation B.4 and B.5 respectively.

$$\frac{\partial T}{\partial t} = \frac{k}{\rho c_p} \nabla^2 T \tag{B.4}$$

$$\frac{\partial c}{\partial t} = D \nabla^2 c \tag{B.5}$$

By comparison, the relationship between diffusion coefficient and effective thermal conductivity is assumed as shown in Equation B.6.

$$\frac{k}{\rho c_p} = D \tag{B.6}$$

In order to make proper substitutions for all the constants, the boundary conditions should also be considered.

$$\text{Thermal flux} \quad J_T = -k \nabla T$$

$$\text{Mass flux} \quad J_M = -D \nabla c \tag{B.7}$$

To obtain the same boundary flux, the thermal conductivity is assumed to be the diffusion coefficient. Meanwhile, Equation B.6 should also be satisfied. Thus,

$$\rho c_p = 1 \tag{B.8}$$

B.2 Diffusion Induced Strain

In order to obtain the equivalent diffusion induced strain by using heat conduction equation, the strain law should adjusted accordingly. By comparing thermal induced strain and mass diffusion induced strain in an isotropic material as shown in Equation B.9, the assumption is given by Equation B.10.

$$\text{Thermal strain} \qquad \varepsilon_{ij}^{ei\_T} = \alpha \Delta T \delta_{ij}$$

$$\text{Mass diffusion induced strain} \qquad \varepsilon_{ij}^{ei\_c} = \frac{1}{3} \Delta c \Omega \delta_{ij} \tag{B.9}$$

$$\alpha = \frac{1}{3}\Omega \tag{B.10}$$

A correspondence between the thermal and mass diffusion parameters is presented in Table B.1.

Table B.1 Correspondence between thermal and mass diffusion parameters

Mass diffusion Parameter		Thermal Parameter		Relationship
Description	Symbol	Description	Symbol	
Thermal conductivity	D	Diffusion coefficient	k	k=D
Density	ρ	Density	ρ	ρ=ρ
-	-	Specific heat capacity	c_p	$c_p = \frac{1}{\rho}$
Mass generation rate per unit volume	$\dot{m}$	Heat generation rate per unit volume	$\ddot{q}$	$\ddot{q} = \dot{m} = 0$
Partial molar volume	Ω	Thermal expansion coefficient	α	α=1/3Ω

APPENDIX C

As introduced in Appendix B, for the 2-D macro-scale 2-D model the thermal module in ANSYS has already been converted into a mass diffusion module to analyze the diffusion induced stress. In order to add temperature change on this converted module, the temperature change should be converted to an effective concentration change to introduce equivalent effects.

As shown in Equation 2.15, to generate the same amount of strain, the relationship between temperature and effective concentration is

$$\frac{1}{3}\Omega\Delta c_{eff} = \alpha_{eff}\Delta T \tag{C.1}$$

where Δc_{eff} is the effective concentration, ΔT is the temperature change, α_{eff} is the effective thermal expansion coefficient. Thermal expansion coefficients of solid electrode particles and electrolytes are different. The effective thermal expansion coefficient for the whole electrode can be obtained by applying the rule of mixture. The effective concentration can be calculated by:

$$\Delta c_{eff} = \frac{3\alpha_{eff}}{\Omega}\Delta T = \frac{3(\alpha_p V_p + \alpha_e V_e)}{\Omega}\Delta T \tag{C.2}$$

It should be noted that the expansion of some the other small parts of the electrodes, like the binders, are neglected.

REFERENCES

REFERENCES

1. M. Silberberg, *Chemistry: The Molecular Nature of Matter and Change*, 4th ed. New York: McGraw-Hill Education, 2006.

2. S. S. Zhang, "Battery Separator", *SciTopics*, July 22, 2008, accessed July 2, 2010, http://www.scitopics.com/Battery_Separator.html.

3. K. Nishio and N. Furukawa, "Practical Batteries", in *Handbook of Battery Materials*, ed. J. O. Besenhard, New York: Wiley-VCH, 1999.

4. L. Gaines and R. Cuenca, "Costs of Lithium-Ion Batteries for Vehicles", accessed August 11, 2010, http://www.transportation.anl.gov/pdfs/TA/149.pdf.

5. M. D. Farrington, "Safety of Lithium Batteries in Transportation", *Journal of Power Sources*, 96, (2001), 260-265.

6. C. Daniel, "Materials and Processing for Lithium-Ion Batteries", *JOM*, Vol. 60 No.9, 2008, http://www.tms.org/pubs/journals/jom/0809/daniel-0809.html.

7. P. Arora and Z. M. Zhang, "Battery separators", *Chem*. Rev. 2004, 104, 4419-4462.

8. S. S. Zhang, "A review on the separators of liquid electrolyte Li-ion batteries", *Journal of Power Sources*, 164 (2007) 351–364.

9. "Products", accessed October 12, 2010, http://www.celgard.com/.

10. "A Rechargeable Lithium-ion Battery Model – Charge and Discharge Behavior", COMSOL, accessed December 2, 2010, http://www.comsol.asia/showroom/gallery/686/.

11. Advisory Notice: "Transportation Of Lithium Batteries", Federal Register, 65, No. 174, (2000), Notice No. P54336.

12. M. Doyle, T.F. Fuller, J. Newman, "Modeling of Galvanostatic Charge and Discharge of the Lithium/Polymer/Insertion Cell", *Journal of the Electrochemical Society*, 140 (1993) 1526–1533.

13. M. Doyle, J. Newman, A.S. Gozdz, C.N. Schmutz and J.M. Tarascon, "Comparison of Modeling Predictions with Experimental Data from Plastic Lithium Ion Cells", *Journal of the Electrochemical Society*, 143 (1996) 1890–1903.

14. J. Christensen and J. Newman, "A Mathematical Model of Stress Generation and Fracture in Lithium Manganese Oxide", *Journal of the Electrochemical Society*, 153 (2006), A1019–A1030.

15. J. Christensen and J. Newman, "Stress Generation and Fracture in Lithium Insertion Materials", *Journal of Solid State Electrochemistry,* 10 (2006) 293–319.

16. X.C. Zhang, W. Shyy and A.M. Sastry, "Numerical Simulation of Intercalation-Induced Stress in Li-Ion Battery Electrode Particles", *Journal of the Electrochemical Society*, 154, (2007) A910–A916.

17. Y.T. Cheng and M.W. Verbrugge, "Evolution of Stress within a Spherical Insertion Electrode Particle under Potentiostatic and Galvanostatic Operation", *Journal of Power Sources,* 190 (2009) 453–460.

18. Y.T. Cheng and M.W. Verbrugge, "The Influence of Surface Mechanics on Diffusion Induced Stresses within Spherical Nanoparticles", *Journal of Applied Physics,* 104, 083521 (2008).

19. M.W. Verbrugge and Y.T. Cheng, "Stress and Strain-Energy Distributions within Diffusion-Controlled Insertion-Electrode Particles Subjected to Periodic Potential Excitations", *Journal of the Electrochemical Society*, 156 (2009), A927–A937.

20. S. Renganathan, G. Sikha, S. Santhanagopalan and R. E. White, "Theoretical Analysis of Stresses in a Lithium Ion cell", *Journal of the Electrochemical Society*, 157 (2) (2010) A155-A163.

21. S. Golmon, K. Maute and M. L. Dunn, "Numerical Modeling of Electrochemical-Mechanical Interactions in Lithium Polymer Batteries", *Computers and Structures,* 87 (2009) 1567–1579.

22. L. Cai and R. E. White, "Mathematical Modeling of a Lithium Ion Battery", Proceedings of the *COMSOL Conference* 2009 Boston.

23. R. E. Garcia, Y.M. Chiang, W.C. Carter, P. Limthongkul and C.M. Bishop, "Microstructural Modeling and Design of Rechargeable Lithium-Ion Batteries", *Journal of the Electrochemical Society*, 152 (2005) A255–A263.

24. X. Xiao, W. Wu and X. Huang, "A Multi-Scale Approach for the Stress Analysis of Polymeric Separators in a Lithium-Ion Battery", *Journal of Power Sources,* 195, (2010), 7649-60.

25. X. C. Zhang, A. M. Sastry and W.Shyy, "Intercalation-Induced Stress and Heat Generation within Single Lithium-Ion Battery Cathode Particles", *Journal of the Electrochemical Society*, 155 (7) (2008) A542-A552.

26. V. Srinivasan and C. Y. Wang, "Analysis of Electrochemical and Thermal Behavior of Li-Ion Cells", *Journal of the Electrochemical Society*, 150 (1) (2003) A98-A106.

27. K. E. Thomas and J. Newman, "Thermal Modeling of Porous Insertion Electrodes", *Journal of the Electrochemical Society,* 150 (2) (2003) A176-A192.

28. W. Wu, X. Xiao and D. Shi, "Heat Transfer and Thermal Stress in a Lithium-Ion Battery", IMECE2010-37870, Proceedings of the *ASME* 2010 Congress, Nov, 2010.

29. M. Alamgir, "Primary & Secondary Batteries – Other Technologies", Presentation at the *26th International Battery Seminar & Exhibit*, March 16-19, 2009, Fort Lauderdale, Florida.

30. K. Kumaresan, G. Sikha, and R. E. White, "Thermal Model for a Li-Ion Cell", *Journal of the Electrochemical Society*, 155 (2) (2008) A164-A171.

31. K. E. Thomas, C. Bogatu and J. Newman, "Measurement of the Entropy of Reaction as a Function of State of Charge in Doped and Undoped Lithium Manganese Oxide", *Journal of the Electrochemical Society*, 148 (6) (2001) A570-A575.

32. S. A. Hallaj, R. Venkatachalapathy, J. Prakash and J. R. Selman, "Entropy Changes Due to Structural Transformation in the Graphite Anode and Phase Change of the LiCoO2 Cathode", *Journal of the Electrochemical Society*, 147 (7) (2000) 2432-2436.

33. R. Deshpande, Y. Qi and Y. T. Cheng, "Effects of Concentration-Dependent Elastic Modulus on Diffusion-Induced Stresses for Battery Applications", *Journal of the Electrochemical Society*, 157 (8) (2010) A967-A971.

34. Products, Timcal Graphite & Carbon, accessed December 1, 2010, http://www.timcal.com/scopi/group/timcal/timcal.nsf.

35. Products, Toda America, accessed December 1, 2010, http://www.todaamerica.com/products/products.html.

36. A. K. Shucla and T. P. Kumar, "Materials for Next Generation Lithium Batteries", *Current Science Association*, 94(3) (2008), pp. 314-331.

37. M. S. Whittingham, "Materials Challenges Facing Electrical Energy Storage", *MRS Bulletin*, 33 (4) (2008), pp.411-419.

38. K. K. Chawla, *Composite Materials Science and Engineering*, New York: Springer-Verlag, 1987.

39. W.D. Callister, *Materials Science and Engineering, an Introduction*, 5th ed, New York: John Wiley & Sons, Inc, 2000.

40. S. J. Harris, A. Timmons, D. R. Baker and C. Monroe, "Direct In-Situ Measurements Of Li Transport in Li-Ion Battery Negative Electrodes", *Chemical Physics Letters*, 485 (2010) 265-274.

41. R. Spotnitz and J. Franklin, "Abuse Behavior of High-Power, Lithium-Ion Cells", *Journal of Power Sources*, 113 (2003) 81–100.

42. "Charging lithium-ion batteries", Battery University, accessed November 14, http://batteryuniversity.com/index.php/learn/article/charging_lithium_ion_batteries;

43. "D10, D50 and D90", accessed November 16, http://www.lactose.com/particle_size/d10_d50_d90.html.

44. “ANSYS Thermal Analysis Guide”, accessed October 21, 2010, http://www1.ansys.com/customer/content/documentation/100/ansys/gthe100.pdf.

45. D. R. Hose, B. Griffiths, S. Mahmood, J. Gunn, D. Sweeney, J. Kelly and P. V. Lawford, “Modelling drug delivery from stents using ANSYS”, accessed July 2, 2010, http://www.technet-alliance.com/uploads/tx_caeworld/drugdelivery.pdf.

46. A. Sheidaei, X, Xiao, J. Wang and X. Huang, “Mechanical Characterization of a Lithium Ion Battery Separator Using a Dynamic Mechanical Analyzer”, *SAE* 2011-PFL-168, Detroit MI, April, 2011.

47. V. B, Shenoy, P. Johari and Y. Qi, “Elastic Softening of Amorphous and Crystalline Li-Si Phases with Increasing Li Concentration: A First-Principles Study”, *Journal of Power Sources*, 195 (2010) 6825–6830.

48. Y. Qi, H. Guo, L.G. J. Hector and A. Timmons, “Three-Fold Increase in the Young's Modulus of Graphite Negative Electrode during Lithium Intercalation”, *J Electrochemical Society*, 157 (2010) A558-566.